Journal of Colloid and Interface Science 633 (2023) 907–922

Contents lists available at ScienceDirect

Journal of Colloid and Interface Science

journal homepage: www.elsevier.com/locate/jcis

Elucidating the nanostructure of small interfering RNA-loaded lipidoid-polymer hybrid nanoparticles

Anas Aljabbari [a,1], Abhijeet Girish Lokras [a,1], Jacob Judas Kain Kirkensgaard [b,c], Thomas Rades [a], Henrik Franzyk [d], Aneesh Thakur [a], Yibang Zhang [e], Camilla Foged [a,*]

[a] Department of Pharmacy, Faculty of Health and Medical Sciences, University of Copenhagen, Universitetsparken 2, 2100 Copenhagen Ø, Denmark
[b] Department of Food Science, Faculty of Science, University of Copenhagen, Rolighedsvej 26, 1958 Frederiksberg C, Denmark
[c] Niels Bohr Institute, University of Copenhagen, Universitetsparken 5, 2100 Copenhagen Ø, Denmark
[d] Department of Drug Design and Pharmacology, Faculty of Health and Medical Sciences, University of Copenhagen, Jagtvej 162, 2100 Copenhagen Ø, Denmark
[e] School of Pharmacy, Jiangsu University, 301 Xuefu Road, Jingkou District, Zhenjiang, Jiangsu 212013, China

GRAPHICAL ABSTRACT

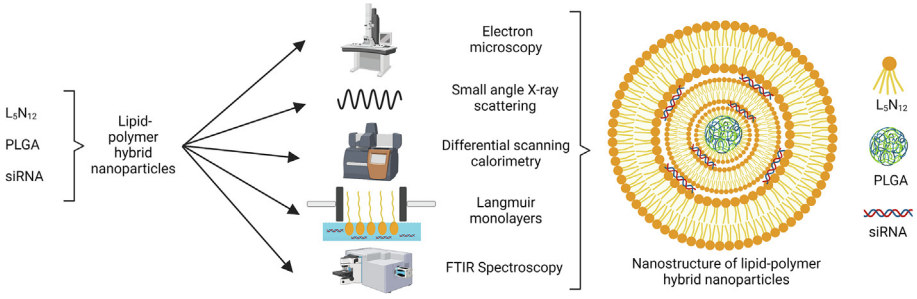

ARTICLE INFO

Article history:
Received 7 June 2022
Revised 21 November 2022
Accepted 27 November 2022
Available online 28 November 2022

Keywords:
Lipidoid-polymer hybrid nanoparticles
siRNA
Lipoplex, nanostructure
Drug delivery
Nanomedicine

ABSTRACT

We analyzed the structural and material properties of small interfering RNA (siRNA)-loaded lipid-polymer hybrid nanoparticles (LPNs) containing ionizable lipidoid and poly(DL-lactic-*co*-glycolic acid) (PLGA) using small-angle X-ray scattering, cryogenic transmission electron microscopy, polarized light microscopy, the Langmuir monolayer methodology, differential scanning calorimetry, and attenuated total reflectance Fourier-transform infrared (ATR-FTIR) spectroscopy. Scattering analyses showed that bulk lipidoid self-assemble into lamellar structures with a *d*-spacing of 38 Å, whereas lipidoid-siRNA lipoplexes display an in-plane lateral organization of siRNA in between lipidoid bilayers with a repeat distance of approximately 55 Å. The siRNA-loaded LPNs adopted a core–shell structure with an interaxial alignment of siRNA between lipidoid shell bilayers. Langmuir monolayer experiments showed a distinct interaction between the lipidoid headgroups and siRNA, which was dependent on buffer subphase pH. Thermal analyses suggested that PLGA and lipidoid interact, which was evident from a shift in the phase transition temperature of lipidoid, and the thermotropic phase behavior of lipidoid was affected by inclusion of siRNA. ATR-FTIR data confirmed the shift or disappearance of characteristic absorption bands of siRNA after lipidoid binding. In conclusion, siRNA-loaded LPNs display a core–shell structure, wherein the polymeric core functions as a colloid matrix support for siRNA-loaded lipidoid shell layers.

* Corresponding author at: Department of Pharmacy, Faculty of Health and Medical Sciences, University of Copenhagen, Universitetsparken 2, DK-2100 Copenhagen Ø, Denmark.
E-mail address: camilla.foged@sund.ku.dk (C. Foged).
[1] These authors contributed equally.

https://doi.org/10.1016/j.jcis.2022.11.141
0021-9797/

1. Introduction

RNA therapeutics, *e.g.*, small interfering RNA (siRNA), represent a research area of rapidly growing interest within both academia and pharmaceutical companies [1]. Nonetheless, the realization of the full potential of RNA therapeutics is highly dependent on the design of safe and efficacious delivery technologies that mediate transport of large and negatively charged RNA molecules across biological membranes into the target cells. Synthetic nanoparticles represent interesting delivery systems that can be customized to: (i) protect the RNA cargo against degradation, (ii) mediate cellular uptake via endocytosis, and (iii) release the RNA cargo into the cytosol after endosomal escape. A prime example is the approved siRNA-based drug Patisiran, which is based on siRNA-loaded lipid nanoparticles (LNPs) [2].

We recently designed an alternative nanocomposite delivery system, *i.e.*, lipid-polymer hybrid nanoparticles (LPNs), composed of so-called lipidoid and poly(D,L-lactic-*co*-glycolic acid) (PLGA) [3]. Lipidoids belong to a novel class of ionizable cationic lipid-like materials that efficiently interact with polyanionic nucleic acids via electrostatic attractive interactions, and mediate cellular uptake, endosomal escape, and cytosolic delivery [4]. The lipidoid analogue referred to as L_5 displays a tetraamine backbone linked to five alkyl chains. The delivery potential of L_5-modified LPNs has been demonstrated both *in vitro* [3] and *in vivo* [5,6]. We hypothesized that PLGA forms the polymeric core of the LPNs enabling a sustained release of siRNA, and it thus constitutes an inherent part of the LPN architecture, whereas L_5 interacts with the PLGA core and forms a membrane shell structure around the core [3,5]. The cationic L_5 headgroups neutralize the anionic charge of the nucleic acid cargo, while the hydrophobic alkyl chains play a role during cell membrane fusion. However, the detailed nanoarchitecture of the siRNA-loaded LPNs remains elusive.

The purpose of the present study was to elucidate the nanostructural and material properties of siRNA-loaded LPNs by using advanced analytical techniques. Small-angle X-ray scattering (SAXS) was applied to resolve the nanoscale repeat structure in the LPNs to gain an understanding of the presence of order in the delivery system. Cryogenic transmission electron microscopy (cryo-TEM) provided high-resolution images of the LPNs in their near-native state to confirm the SAXS patterns. The Langmuir monolayer methodology and differential scanning calorimetry (DSC) were applied to study the physical interaction between the siRNA cargo and the ionizable lipid. Finally, attenuated total reflectance Fourier-transform infrared (ATR-FTIR) spectroscopy was used to investigate chemical interactions between the different LPN constituents. To facilitate structural analysis, we synthesized an array of L_5 analogues with systematically increased alkyl chain length (12, 14 and 16 carbon atoms) denoted L_5N_{12}, L_5N_{14}, and L_5N_{16}, respectively. The properties of these compounds were analyzed in bulk, as well as upon incorporation into siRNA lipoplexes and siRNA-loaded LPNs.

2. Materials and methods

2.1. Materials

2′-*O*-methyl-modified dicer substrate asymmetric siRNA duplex directed against tumor necrosis factor α (TNF-α siRNA, 17928.334 g/mol) was kindly provided as a dried, purified, and desalted duplex by GlaxoSmithKline (Stevenage, UK). The TNF-α siRNA consisted of the following sequences: TNF-α sense 5′-pGUCUCAGCCUCUUCUCAUUCCUGct-3′, and antisense 5′-AGCAGGAAUGAGAAGAGGCUGAGACAU-3′, where the underlined capital letters represent 2′-*O*-methylribonucleotides, lowercase letters represent deoxyribonucleotides, and p represents a phosphate residue. The duplex was re-annealed in a buffer consisting of 30 mM 4-(2-hydroxyethyl)-piperazine-1-ethanesulfonic acid (HEPES) and 100 mM potassium acetate (to give pH 7.5). L_5N_{12} was synthesized, purified, and characterized as reported previously [3,7]. PLGA (lactide:glycolide molar ratio 75:25, average MW: 20 kDa) was purchased from Wako Pure Chemical Industries (Osaka, Japan). Poly(vinyl alcohol) (PVA) 403 with an 87–90 % degree of hydrolysis was procured from Sigma-Aldrich (St. Louis, MO, USA). Quant-iT™ RiboGreen® RNA Reagent and Tris–EDTA buffer (10 mM Tris, 1 mM EDTA, pH 8.0) (TE buffer) were acquired from Molecular Probes, Invitrogen (Paisley, UK). All chromatographic mobile phases were obtained by mixing solvents from VWR (Radnor, PA, USA).

2.2. Synthesis of L_5N_{14} and L_5N_{16}

The synthesis of L_5N_{14} and L_5N_{16} is described in the Supporting Information (Figs. S1 and S2). The identity and purity of the compounds were confirmed by using high performance liquid chromatography and mass spectrometry, respectively (Supporting Information, Tables S1–S4 and Figs. S3–S7).

2.3. Preparation of fully hydrated bulk dispersions, non-loaded liposomes, and lipoplexes

Fully hydrated bulk L_5 analogue dispersions in Tris buffer were prepared and equilibrated as previously described [8]. The final lipid concentration was 25–100 mg/mL. Non-loaded L_5N_{12} liposomes were prepared using the Nanoassemblr Ignite system (Precision Nanosystems, Vancouver, Canada). The organic phase consisted of 3.75 mg L_5N_{12} dissolved in 0.5 mL 0.72 % (v/v) glacial acetic acid prepared in ethanol at a concentration of 7.5 mg/mL. The aqueous phase consisted of 1.5 mL 50 mM NaOAc buffer (pH 5.2). The liposomes were prepared by injecting the organic phase into the first inlet and the aqueous phase into the second inlet of the microfluidic mixing cartridge. The total flow rate (TFR) and the flow rate ratio (FRR) were kept constant at 12 mL/min and 3:1 (v/v, aqueous to organic phase), respectively, to produce liposomes with a final lipid concentration of 3.75 mg/mL. For preparation of siRNA-L_5N_{12} lipoplexes, a stock solution of 30 mg/mL L_5N_{12} was prepared by dissolving L_5N_{12} in a mixture of 30 μL trifluoroacetic acid and 170 μL dimethyl sulfoxide, as previously described [3]. Consequently, 90, 45, and 30 μL, respectively, of this stock solution were mixed vigorously with 10 μL (180 μg) 18 mg/mL TNF-α siRNA solution in 2 mL RNase-free glass vials to prepare L_5N_{12}:TNF-α siRNA lipoplexes at weight ratios of 15:1, 7.5:1, and 5:1, respectively. In addition, L_5N_{14} and L_5N_{16} lipoplexes were prepared in the same way at a weight ratio of 15:1. Throughout the study, we have chosen to use weight ratios, and not amine-to-phosphate (N/P) ratios, which are commonly used to indicate the ratio between the number of positively charged amine groups and the number of negatively charged phosphate groups. The reason for this is that the lipidoid headgroups contain multiple secondary and tertiary amine groups displaying different pK_a values, which makes estimation of headgroup charge highly challenging.

2.4. Preparation of non-loaded and siRNA-loaded lipidoid-polymer hybrid nanoparticles

LPNs were prepared by using the double emulsion solvent evaporation technique, as previously described [7]. In brief, the water phase (w_1) was composed of 150 μg TNF-α siRNA dissolved in 125 μL TE-buffer for the siRNA-loaded LPNs, whereas TE-buffer alone was used for preparation of non-loaded LPNs. Subsequently, w_1 was added to 250 μL oil phase (o_1) consisting of L_5 and PLGA at

different weight ratios in CH_2Cl_2 at a constant concentration of solids (60 mg/mL), eventually resulting in the formation of a primary emulsion, which was sonicated with a probe tip sonicator (QSonica, Newtown, CT, USA) for 90 s at 50 % amplitude. A volume of 1 mL 2 % (w/v) PVA solution was subsequently added to the emulsion as the second water phase (w_2), which was vortexed for 1 min, thereby creating a phase inversion resulting in a water-in-oil-in-water ($w_1/o_1/w_2$) double emulsion. This emulsion was sonicated for 90 s at 30 % amplitude, and was subsequently poured into a 25-mL glass beaker with a stirring bar. The vial was rinsed with 2 × 2 mL 2 % (w/v) PVA solution, which was added to the beaker, along with a final addition of 1 mL 2 % (w/v) PVA solution. The content of the beaker was stirred for 45 min, allowing the CH_2Cl_2 to evaporate, and the LPNs to form. The resulting dispersion was then transferred into three 2-mL centrifuge tubes. The dispersion was purified by centrifugation (Optima™ Max Ultracentrifuge, Beckman Coulter, Brea, CA, USA) using the following sequence of centrifugal forces at 4 °C: 6000*g* for 5 min, 12,000*g* for 5 min, 21,000*g* for 5 min, 34,000*g* for 5 min, and finally 48,000*g* for 10 min. The supernatant containing un-encapsulated siRNA was discarded after each centrifugation step, and the nanoparticle pellet was re-dispersed in 2 mL DEPC-treated water. The siRNA-loaded LPNs were prepared at different weight ratios of L_5N_{12}:PLGA and L_5N_{12}:siRNA to study the structural effect of these ratios on the resulting formulation. For example, for the formulation prepared at 15 % (w/w) L_5N_{12}:PLGA and 15:1 (w/w) L_5N_{12}:siRNA, 2.25 mg L_5N_{12}, 12.75 mg PLGA, and 150 μg siRNA were used.

2.5. Size, polydispersity index (PDI), zeta potential, and encapsulation efficiency

Dynamic light scattering was used to determine the hydrodynamic size (*z*-average) and polydispersity index (PDI) of the nanoparticles, while the zeta potential and encapsulation efficiency were determined by using laser Doppler microelectrophoresis and fluorescence spectroscopy, respectively, as reported previously [3]. Briefly, samples (diluted to approx. 0.3 mg/mL solid content) were analyzed at 25 °C employing a Zetasizer Nano ZS (Malvern Instruments, Worcestershire, UK) equipped with a 633 nm laser and 173° detection optics. For measurement of the encapsulation efficiency, a volume of 25 μL LPN dispersion was centrifuged at 22,000*g* (4 °C), a volume of 200 μL $CHCl_3$ was added, and the pellet was resuspended by brief vortexing. A volume of 475 μL HD solution, composed of 100 μM octyl glucoside (OG) and 1 mg/mL heparin, was added to the $CHCl_3$ mix, and vortexed for 1 min. The resulting mixture was rotated end-over-end for 5 min for efficient extraction of siRNA into the aqueous phase. Subsequently, the two phases were separated by centrifugation at 4 °C and 22,000*g* for 10 min. The supernatant (aqueous phase) was isolated, diluted with TE buffer, and incubated at 37 °C to evaporate residual $CHCl_3$. The siRNA concentration in the samples was analyzed using the RiboGreen® RNA reagent according to the manufacturer's instructions employing a fluorescence plate reader (FLUOstar OPTIMA, BMG Labtech, Ortenberg, DE). The excitation and emission wavelengths were set at 485 nm and 520 nm, respectively.

2.6. Small-angle X-ray scattering (SAXS)

The experiments were performed using a Ganesha SAXS system (SAXSLab, Kongens Lyngby, Denmark) essentially as described previously [8], with minor modifications. The instrument was equipped with a 100XL+ microfocus sealed X-ray tube (Rigaku, Tokyo, Japan), producing a beam with a wavelength of 1.54 Å. The scattering patterns were recorded with a two-dimensional 300 K Pilatus pixel area detector (Dectris, Baden, Switzerland). A *q*-range spanning from 0.02 to 1.0 $Å^{-1}$ was used. Silver behenate [$H_3C(CH_2)_{20}COOAg$] with a *d*-spacing value of 58.38 Å was used as a standard to calibrate the angular scale for the small-angle setting [9]. For peaks that were less well defined, the highest and most central point of the peak was assigned as the peak position.

2.7. Cryogenic transmission electron microscopy (cryo-TEM)

Morphological analysis was carried out by cryo-TEM using a Tecnai G2 20 TWIN transmission electron microscope (FEI, Hillsboro, OR, USA), as previously described [3]. The samples were prepared by using a FEI Vitrobot Mark IV™ (Thermo Fischer Scientific, Waltham, MA, USA) by adding 2 μL formulation onto a Pelco Lacey carbon-filmed grid to form a thin film of approximately 10–500 nm. Subsequently, the grid was plunged into liquid ethane and transferred in liquid N_2 to an Oxford CT3500 cryo holder connected to the electron microscope. The samples were visualized in the bright field mode at an acceleration voltage of 120 kV. Images were captured with a Gatan imaging filter 100 CCD camera (Gatan, Pleasanton, CA, USA).

2.8. Polarized light microscopy

The L_5 analogues were dissolved in $CHCl_3$ at a concentration of 100 mg/mL. A volume of 5 μL was placed on a microscopy slide and left to evaporate for 2 h. The films were subsequently rehydrated with 5 μL DEPC water, and cover slips were placed on the samples, which were imaged with a Leica DM light microscope (Wetzlar, Germany), equipped with a polarizing and an analyzing filter, respectively. The magnification was pre-set to 50×, and images were captured at an exposure time of 2000 ms.

2.9. Langmuir monolayers

Monolayers of neat L_5 analogues were formed at 22 °C by spreading a total amount of 14.85 nmol lipid in $CHCl_3$ on 175 mL Tris buffer (pH 7.4) and NaOAc buffer (pH 5.2) subphases, respectively, in a KSV Minitrough 1 (KSV Instruments ltd., Helsinki, Finland) with a surface area of 243 cm^2 by using a Hamilton micro syringe. This corresponds to 0.06 nmol L_5 analogue per cm^2 before compression. The monolayers were compressed as previously described [10]. The surface pressure (Π) was measured as a function of the mean molecular area (A) by using a Wilhelmy platinum plate (KSV Instruments ltd.). Each sample was compressed once in three independent experiments ($N = 3$). The KSV NIMA LB software (v 3.80) and Microsoft Excel were used for data analysis. The phase transitions and collapse points were estimated from the compression modulus (Cs^{-1}) versus Π dependency, where $Cs^{-1} = -A(d\Pi/dA)$. A characteristic minimum for the C_S^{-1} versus Π dependency for the monolayer reflects the phase transition from the liquid-expanded (LE) to the liquid-condensed (LC) states of the monolayer, whereas the Π-value at $(d\Pi/dA) = 0$ identifies the point of the monolayer collapse [11]. To further characterize the monolayers, the isotherms were processed to obtain the following parameters: The mean molecular area at the collapse point ($A_{collapse}$), and the limiting molecular area (A_{lim}), which represents the headgroup area occupied by one molecule when the monolayer is in an apparent solid (S) phase. A_{lim} was used to calculate the critical packing parameter (*CPP*), which is given by equation 1:

$$CPP = \frac{v}{A_{lim} \times l}$$

where v is the volume of the hydrophobic moiety, and l is the effective chain length. The values for v and l were calculated based on the number of carbon atoms in the lipid chain, as reported previ-

ously [12]. A_{lim} was calculated by extrapolating the apparent S phase of the isotherm to the x-axis by using linear regression [13]. Linearity was assessed as a function of the R^2 value from the maximum number of data points (>35) and was found to be >0.998.

2.10. Differential scanning calorimetry (DSC)

Thermal analysis of the liquid formulations was performed by using a NanoDSC (TA Instruments, Newcastle, DE, USA). A sample volume of 300 µL was used. The scanning rate was set to 0.5 °C/min within a temperature range of 20–70 °C, and each sample was analyzed in three consecutive runs (n = 3). A representative scan for each formulation was used for data analysis. The phase transition temperature (T_m) was determined, and the change in enthalpy (ΔH) was assessed by integrating the area under the baseline-corrected excess heat capacity (C_p) curve obtained for each sample.

2.11. Attenuated total reflectance Fourier-transform infrared (ATR-FTIR) spectroscopy

Samples were concentrated by solvent evaporation after depositing solutions onto the surface of a silicon crystal. FTIR spectra between 800 and 3500 cm^{-1} of the highly concentrated samples were collected at room temperature by using a Bomem MB 104 IR spectrometer (ABB, Bomem, Quebec, Canada) in ATR mode. Each spectrum was recorded by collecting 128 scans at a resolution of 2 cm^{-1}.

2.12. Statistics

Data was analyzed by using the GraphPad Prism software (Version 6, La Jolla, CA, USA). Statistically significant differences were assessed by using ANOVA followed by a Tukey's post-hoc multiple comparison test. A p-value $\leq$ 0.05 was considered statistically significant.

3. Results

3.1. Preparation of formulations and initial physicochemical characterization

The hydrodynamic diameter (z-average), PDI, zeta potential, and siRNA encapsulation efficiency for the siRNA-loaded LPNs, as well formulations prepared for control purposes, were measured (Table S5). All LPN formulations displayed similar size profiles within the range of 180–210 nm with relatively low PDI values of 0.06–0.15, as previously reported [3,5,14]. The zeta potential varied, with L_5N_{12}-modified LPNs displaying a zeta potential of + 19 mV, while L_5N_{14}-modified and L_5N_{16}-modified LPNs had significantly lower zeta potentials of + 6 mV (p < 0.01) and −16 mV (p < 0.001), respectively. We hypothesize that this difference in zeta potential might be caused by a chain length-dependent difference in the surface pK_a values of the lipid amine headgroups. Hence, with longer chain length, the ability to remove a proton in the amine headgroup increases, and, consequently, the surface pK_a value decreases. In this way, the resulting zeta potential will decrease with increasing chain length. Such chain length-dependence has been reported for the surface pK_a of saturated carboxylic acids in monolayers at the air–water interface, displaying alkyl chain lengths from six to sixteen carbon atoms [15]. The siRNA encapsulation efficiency was approximately 70 % for all LPN formulations, as reported previously [14]. The HPLC chromatograms of LPNs showed two distinct peaks, corresponding to PLGA and L_5N_{12} (Fig. S8). Hence, the chromatograms confirm the presence of the two main components in the LPNs after ultracentrifugation. In addition, we have recently shown that siRNA molecules encapsulated into LPNs are chemically intact [16] and functional *in vitro* [3] and *in vivo* [6].

3.2. Fully hydrated L_5N_{12} self-assembles into a lamellar phase

Fully hydrated bulk L_5N_{12} dispersions were studied by using SAXS to characterize the structural properties of the self-assemblies as a function of the lipid concentration. The scattering pattern for the fully hydrated L_5N_{12} dispersions displayed an increase in scattering intensity (I) at increasing concentration (Fig. 1A). The repeat distance, calculated from the q_1-value of the main peak at 0.1645 $Å^{-1}$, corresponds to 38 Å, and was independent of concentration in the examined concentration range. A second order peak at a q-value corresponding to 2 × q_1 (0.3271 $Å^{-1}$) was observed only at the highest tested concentration of 100 mg/mL. Hence, these two reflections correspond to a lamellar phase, where L_5N_{12} molecules assemble as bilayers, separated by a water layer, which is evident from the swelling of L_5N_{12} in dispersion, owing to the amphiphilic nature of lipidoids (Fig. 1B). The repeat distance of 38 Å, as calculated from the curve, corresponds to the total thickness of a bilayer and a water layer (Fig. 1B). The presence of a lamellar phase was confirmed by using polarized light microscopy (Fig. 1C). Images of L_5N_{12} showed a high degree of birefringence, as well as the characteristic Maltese crosses, which indicate the formation of concentric lipid bilayers (Fig. 1C).

3.3. Complexation of L_5N_{12} with siRNA results in an in-plane lateral organization of siRNA in between lipidoid bilayers

Subsequently, non-loaded L_5N_{12} liposomes and L_5N_{12} lipoplexes with siRNA at three different L_5N_{12}:siRNA weight ratios (15:1, 7.5:1, and 5:1) were analyzed using SAXS. The non-loaded L_5N_{12} liposomes displayed a scattering pattern characterized by weak, diffuse, and broad peaks, reflecting the form factor of unilamellar vesicles (Fig. 2A). This was confirmed by cryo-TEM imaging of non-loaded L_5N_{12} liposomes that showed non-uniform and flexible unilamellar vesicles, which were translucent due to the low electron density of L_5N_{12} (Fig. 2B). In contrast, lipoplexes displayed scattering patterns characterized by a single peak at a q-value of 0.1135 $Å^{-1}$, corresponding to a repeat distance of approx. 55 Å, which increased in intensity when the L_5N_{12}:siRNA weight ratio was reduced from 15:1 to 5:1 (Fig. 2C). This pattern is most likely the result of siRNA-induced swelling of the water phase between two adjacent lipid bilayers, forming a lateral lamellar phase (Fig. 2D). Furthermore, cryo-TEM images of the lipoplexes prepared at an L_5N_{12}:siRNA ratio of 7.5:1 (w/w) showed spherical unilamellar and multilamellar vesicles comprised of one or several concentric bilayers encapsulating an electron-dense water core (Fig. 2E and 2F), and the bilayers displayed a higher electron density than liposome bilayers (Fig. 2B), indicating the presence of electrostatically adsorbed siRNA. A bilayer thickness of approx. 35 Å was estimated by using ImageJ analysis of the micrograph, which is slightly smaller than the repeat distance measured for the fully hydrated L_5N_{12} dispersions (38 Å, Fig. 1).

3.4. LPNs display a core–shell structure with an interaxial alignment of siRNA between lipidoid shell bilayers

First, the scattering pattern of non-loaded L_5N_{12}-modified LPNs was determined at four different L_5N_{12} contents (Fig. 3A). There was an apparent shift in the q-value towards the lower q-range when the L_5N_{12} content was increased, which indicates an increase in repeat distance. The calculated q-values and repeat distances seen at L_5N_{12} contents of 5, 10, 20, and 25 % in non-loaded LPNs

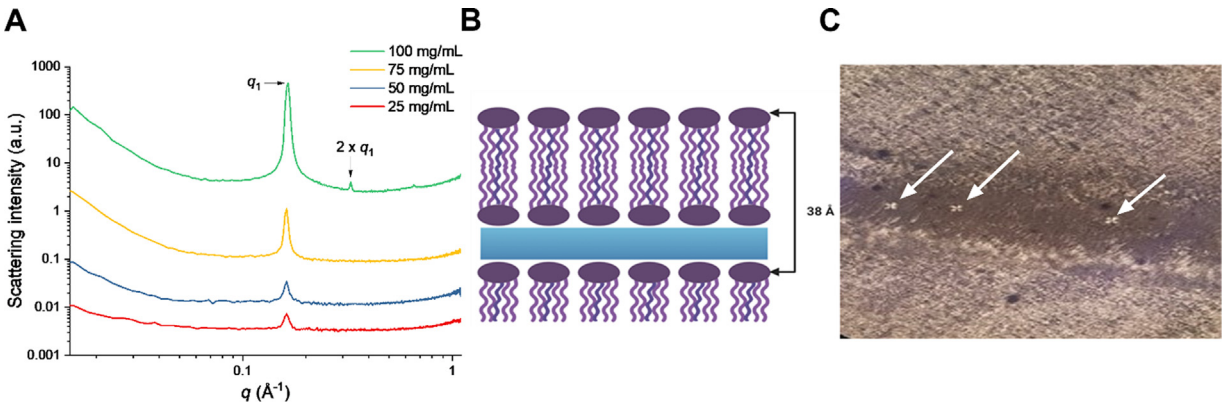

Fig. 1. Structural properties of bulk L_5N_{12} dispersions. **A:** Representative SAXS diffraction patterns of bulk L_5N_{12} dispersed in TE buffer (pH 7.4) at four different concentrations at 20 °C. One reflection at a q-value of 0.1645 Å^{-1}, corresponding to a repeat distance of 38 Å, is evident at 25 mg/ml (red), 50 mg/ml (blue), and 75 mg/ml (yellow), whereas two reflections corresponding to a lamellar phase, also with a repeat distance of 38 Å, are evident at 100 mg/ml (green). The scattering intensity on the y-axis has been shifted vertically for improved visibility. **B:** Graphical representation of the water layer in between L_5N_{12} bilayers. The purple ovals represent the hydrophilic headgroups, and the lipid chains are shown in light purple. The solid blue area represents the water layer. **C:** Representative polarized light microscopy image of bulk L_5N_{12} rehydrated in TE buffer showing birefringence. The arrows mark Maltese crosses, which are characteristic of a lamellar phase of concentric bilayers. Image B was created with BioRender.com. (For interpretation of the references to colour in this figure legend, the reader is referred to the web version of this article.)

were 0.056 Å^{-1}, 0.049 Å^{-1}, 0.044 Å^{-1}, and 0.041 Å^{-1}, and 112 Å, 128 Å, 142 Å, and 153 Å, respectively. The non-loaded LPNs with the highest lipidoid content (25 %) showed the largest repeat distance of 153 Å. In addition, the scattering curves for non-loaded LPNs with an L_5N_{12} content of 20 % and 25 % displayed a second order peak, corresponding to 2 × q_1, which represents a neat lamellar phase. This second order reflection was not evident for non-loaded LPNs with an L_5N_{12} content of 5 % or 10 %. The reason for this could be lack of bilayer structure(s) surrounding the PLGA core when the L_5N_{12} content is reduced, eventually resulting in a structure where L_5N_{12} molecules on the PLGA particle surface are embedded in the polymeric matrix through hydrophobic interactions with the alkyl chains. Alternatively, it could be due to a weaker signal as a result of the lower L_5N_{12} content. The data also suggest that siRNA is not essential for the formation of this general core–shell nanoparticle structure.

Next, we investigated how the loading with siRNA affects the structure of LPNs by preparing siRNA-loaded, L_5N_{12}-modified LPNs at varying L_5N_{12} content (*i.e.*, 5 %, 10 %, 12.5 %, 15 %, 20 %, 25 %, 30 %, 50 % and 70 %: Fig. 3B) at a constant L_5N_{12} to siRNA ratio of 15:1. Increasing the L_5N_{12} content at a constant L_5N_{12}:siRNA ratio also results in an increase in the content of siRNA in the formulation. A peak displaying a q-value almost identical to the q-value (0.1135 Å^{-1}) of the peak for the lipoplexes (Fig. 2C) was observed when the L_5N_{12} content was increased. This peak is evident in the scattering pattern at an L_5N_{12} content of 20 % and above, corresponding to a repeat distance of approx. 55 Å. A shift in the q-value was observed for siRNA-loaded LPNs as the L_5N_{12} content was increased, indicating an increase in repeat distance. This increase plateaued at an L_5N_{12} content of 25 % and higher. The calculated q-values and repeat distances at 10, 12.5, 15, 20, 25, 30, 50, and 70 % L_5N_{12} content in siRNA-loaded LPNs were 0.051 Å^{-1}, 0.050 Å^{-1}, 0.047 Å^{-1}, 0.043 Å^{-1}, 0.039 Å^{-1}, 0039 Å^{-1}, 0.040 Å^{-1}, and 0.038 Å^{-1}, and 123 Å, 125 Å, 136 Å, 146 Å, 161 Å, 161 Å, 157 Å, and 165 Å, respectively (Fig. S9). The difference between the formulations with L_5N_{12} contents of 10 % and 12.5 % is subtle, while the difference was more pronounced at an L_5N_{12} content of 15–25 %. At an L_5N_{12} content higher than 25 %, the q-values are almost constant. For siRNA-loaded LPNs with a lipidoid content of 15 % or higher, a second order reflection was apparent corresponding to 2 × q_1, which indicates the presence of a neat lamellar phase. However, this second order reflection could not be observed for the siRNA-loaded LPNs with a lower L_5N_{12} content.

Cryo-TEM images of siRNA-loaded, L_5N_{12}-modified LPNs displayed spherical nanoparticles with an electron-dense core (Fig. 3C). However, this density is accentuated by the size of the nanoparticles, becoming darker as the size increases, suggesting that this factor might contribute to the observed density (in terms of electron beam penetration). Some nanoparticles displayed distinct structures on the surface, observed as variations in contrast (Fig. 3C). However, whether these can be interpreted as bilayers or simply artefacts of the image remain unclear. Cryo-TEM images of the siRNA-loaded, L_5N_{12}-modified LPNs prepared with 70 % L_5N_{12} content suggest a heterogeneous mixture of non-loaded liposomes, lipoplexes, and LPNs (Fig. 3D and 3E). The LPNs formed were less uniform, and appeared less ordered than the LPNs with lower L_5N_{12} content. However, the electron-dense core of the LPNs indicates that PLGA may be present, as the core displays different electron density. The dense core of the LPNs appear to be surrounded by concentric L_5N_{12} bilayers. Image analysis of the micrographs revealed that the bilayer and water layer thickness is much larger than that observed for lipoplexes. Distances ranged from 110 to 130 Å, which nevertheless were smaller than those calculated from the SAXS data. However, the broadness of the scattering peak suggests that this calculated distance may lack accuracy. The increased combined thickness of the bilayer and the water layer seems largely to arise from an enlargement of the water layer.

Next, the effect of L_5N_{12}:siRNA ratio on the scattering pattern of siRNA-loaded LPNs was investigated. To this aim, siRNA-loaded LPNs were prepared at L_5N_{12}:siRNA ratios of 5:1, 10:1, 15:1 and 20:1, respectively, and subsequently analyzed by SAXS (Fig. 3F). The repeat distance associated with the main peak of the formulations remained constant at 130 Å (q-value of ~ 0.048 Å^{-1}), independently of the L_5N_{12}:siRNA ratio. The appearance of a second order reflection of a lamellar phase is only evident at an L_5N_{12}:siRNA ratio of 15:1, while a peak at a q-value of 0.119 Å^{-1} (repeat distance of 53 Å) appears as the siRNA content increases, relative to the L_5N_{12} content, at ratios of 10:1 and 5:1, presumably caused by interaxial alignment of siRNA.

3.5. Increasing the L_5 chain length results in increased bilayer thickness

To test the effect of chain length, lipoplexes composed of L_5N_{14} and L_5N_{16}, respectively, were prepared at a lipidoid:siRNA ratio of 15:1 (w/w), for comparison with the L_5N_{12} lipoplexes. The scattering patterns for the more hydrophobic L_5N_{14} and L_5N_{16} lipoplexes

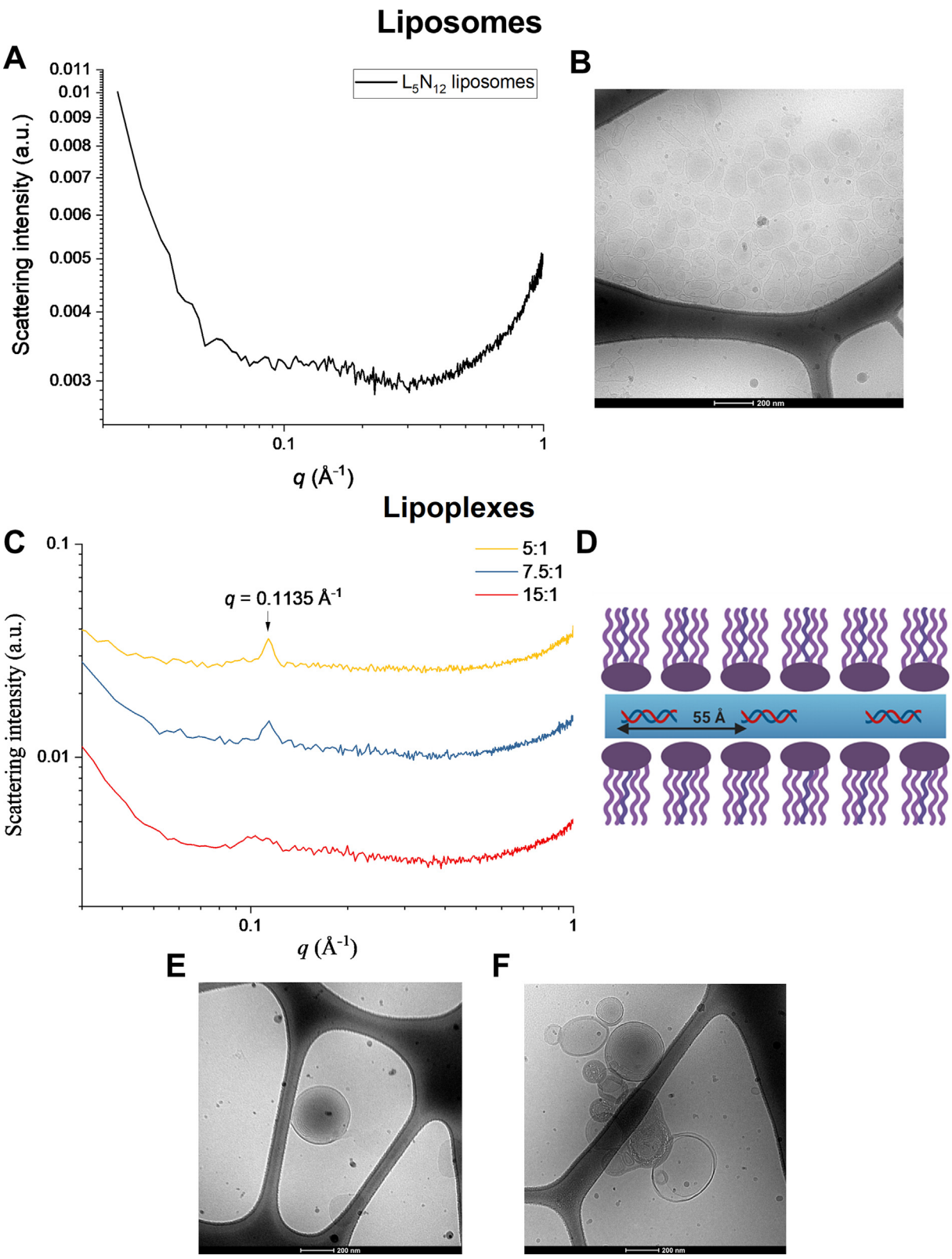

Fig. 2. Structural properties of non-loaded L_5N_{12} liposomes and L_5N_{12}:siRNA lipoplexes. **A:** Representative SAXS diffraction pattern of non-loaded L_5N_{12} liposomes (prepared by using microfluidic mixing) in NaOAc buffer (pH 5.2) at 20 °C. **B:** Representative cryo-TEM image of non-loaded L_5N_{12} liposomes in NaOAc acetate buffer. The image shows flexible and non-spherical liposomes that are translucent, owing to the relatively low electron density of L_5N_{12}. **C:** Representative SAXS diffraction patterns of L_5N_{12}-siRNA lipoplexes in TE buffer (pH 8.0) at 20 °C at L_5N_{12}:siRNA weight ratios of 15:1 (red), 7.5:1 (blue), and 5:1 (yellow), respectively. One distinct reflection at a q-value of 0.1135 Å^{-1}, corresponding to a neat in-plane repeat distance of 55 Å between siRNA molecules in between lipid bilayers, is evident for the ratios 7.5:1 and 5:1. The scattering intensity on the y-axis has been shifted vertically for improved visibility. **D:** siRNA molecules are sandwiched in between lipid bilayers, with an in-plane 55 Å repeat distance between them. **E-F:** Representative cryo-TEM images of L_5N_{12}-siRNA lipoplexes at an L_5N_{12}:siRNA ratio of 7.5:1 (w:w). Image 2D was created using BioRender.com. (For interpretation of the references to colour in this figure legend, the reader is referred to the web version of this article.)

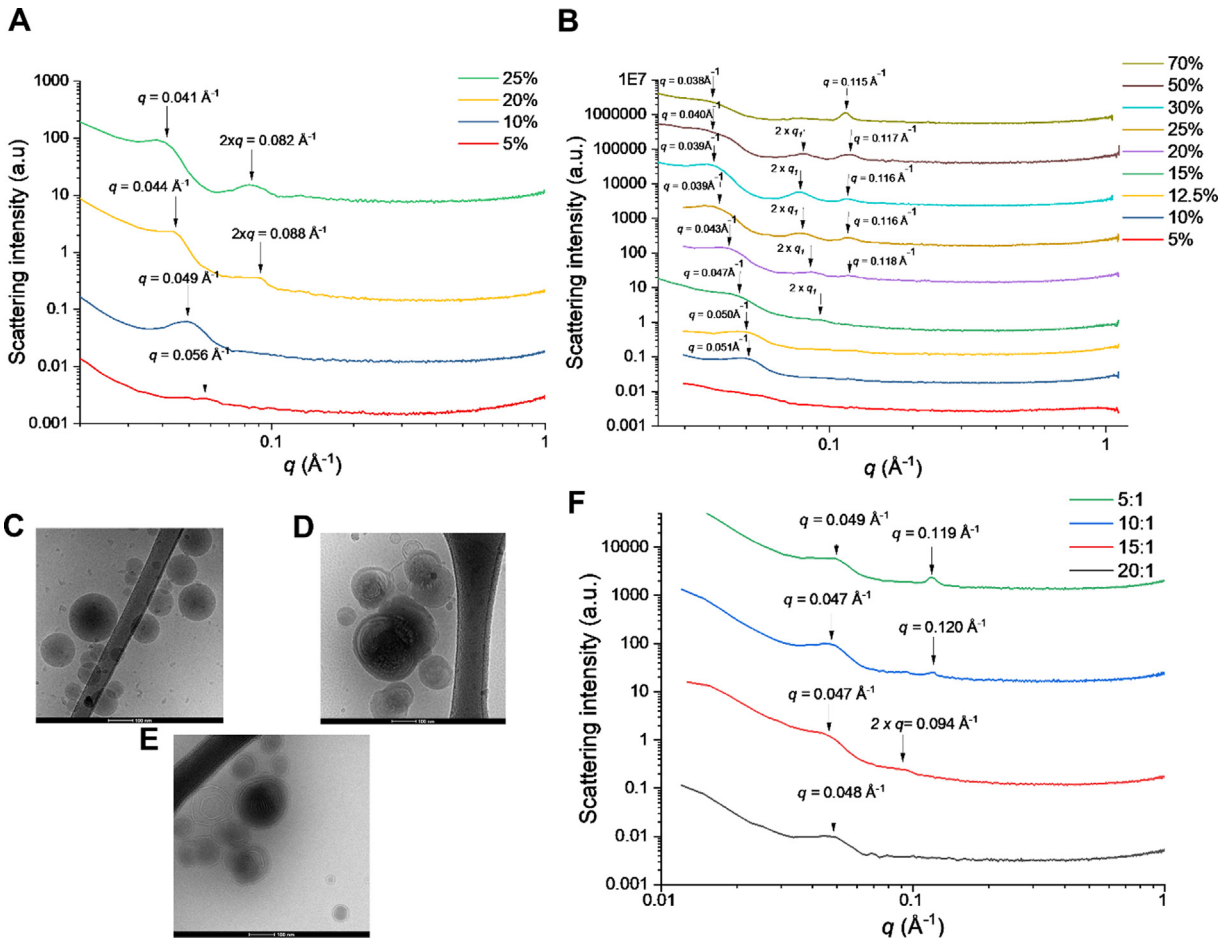

Fig. 3. A: Representative X-ray scattering patterns of non-loaded LPN formulations with varying L_5N_{12} content of 5 % (red), 10 % (blue), 20 % (yellow), and 25 % (green) in DEPC water at 20 °C. The reflections apparent for the 25 % L_5N_{12} content at 0.041 $Å^{-1}$ and the second order reflection at 0.083 $Å^{-1}$ indicate a lamellar phase. The same phase is evident at an L_5N_{12} content of 20 % at *q*-values of 0.044 $Å^{-1}$ and 0.088 $Å^{-1}$, respectively. The scattering patterns for non-loaded LPNs with 5 % and 10 % L_5N_{12} content show only one peak at 0.049 $Å^{-1}$ and 0.056 $Å^{-1}$, respectively. Hence, there is a shift in the *q*-value as the L_5N_{12} content increases. The scattering intensity on the y-axis has been shifted vertically for better visibility. **B:** Representative X-ray scattering pattern of siRNA-loaded LPNs with constant siRNA:L_5N_{12} ratio and varying L_5N_{12} content of 5 % (red), 10 % (blue), 12.5 % (yellow), 15 % (green), 20 % (purple), 25 % (orange), 30 % (cyan), 50 % (brown), and 70 % (olive), analyzed at 20 °C in DEPC water. For each peak, the reflection is marked with an arrow. First and second order reflections for a lamellar phase are apparent for siRNA-loaded LPNs with L_5N_{12} contents of 15 %, 20 %, 25 %, 30 and 50 %, respectively, but not for siRNA-loaded LPNs with L_5N_{12} contents below 15 % or at 70 %. As the L_5N_{12} content increases, a new reflection appears at *q*-values of ~0.117 $Å^{-1}$, corresponding to a repeat distance of ~55 Å, presumably caused by interaxial alignment of siRNA. **C:** Representative cryo-TEM image of siRNA-loaded, L_5N_{12}-modified LPNs prepared at an L_5N_{12}:siRNA ratio of 15:1 and an L_5N_{12} content of 15 % (w/w). **D-E**: Representative cryo-TEM images of siRNA-loaded, L_5N_{12}-modified LPNs prepared at an L_5N_{12}:siRNA ratio of 15:1 and an L_5N_{12} content of 70 % (w/w). **F:** Representative X-ray scattering patterns of siRNA-loaded LPNs with varying L_5N_{12}:siRNA ratio of 20:1 (black), 15:1 (red), 10:1 (blue), and 5:1 (green), analyzed at 20 °C in DEPC water. The reflections are marked for each peak. The first and second order reflections of a lamellar phase can be observed for siRNA-loaded LPNs with an L_5N_{12}:siRNA ratio of 15:1, but not for all other ratios. As the siRNA content increases relative to the L_5N_{12} content, a new reflection at a *q*-value of ~0.119 $Å^{-1}$, corresponding to a repeat distance of 53 Å, may arise from interaxial alignment of siRNA. (For interpretation of the references to colour in this figure legend, the reader is referred to the web version of this article.)

did not show any apparent peaks (Fig. 4A), hence suggesting a lack of repeated structure. Physical observation of L_5N_{16} lipoplexes showed aggregation of lipidoid, suggesting that the protocol used for preparation may be suboptimal for this analogue. To study the effect of chain length on the structure of siRNA-loaded LPNs, siRNA-loaded LPNs containing L_5N_{12}, L_5N_{14} and L_5N_{16}, respectively, were prepared at an L_5:siRNA ratio of 15:1 (w/w) with a total L_5 content of 15 % and a PLGA content of 85 %. The scattering patterns for all three formulations displayed a broad main peak, whereas siRNA-loaded L_5N_{12}- and L_5N_{16}-containing LPNs also showed a second order reflection corresponding to $2 \times q_1$, eventually representing a neat lamellar phase (Fig. 4B). However, this second order lamellar reflection was not evident for siRNA-loaded LPNs containing L_5N_{14}. In addition, there was a clear trend towards increased repeat distance as the L_5 chain length was increased. The calculated *q*-values and repeat distances for L_5N_{12}, L_5N_{14}, and L_5N_{16} LPNs were 0.046 $Å^{-1}$, 0.038 $Å^{-1}$, and 0.032 $Å^{-1}$, and 136 Å, 165 Å, and 196 Å, respectively. Hence, these data confirm that increasing the chain length leads to an increase in bilayer thickness, as expected. Cryo-TEM images of siRNA-loaded L_5N_{16}-based LPNs showed a similar spherical nanoparticle structure with a more uniform electron density throughout the particle (Fig. 4C). For these siRNA-loaded, L_5N_{16}-modified LPNs, clear concentric lipid bilayers were observed, surrounding an electron-dense core. Furthermore, the siRNA-loaded, L_5N_{16}-modified LPNs displayed channel-like structures penetrating the LPNs, rather than shell structures surrounding the nanoparticle core, giving rise to a ball of yarn-like structure.

3.6. The pH of the subphase affects L_5 monolayers

To investigate the effect of pH on L_5N_{12}, L_5N_{14}, and L_5N_{16} monolayers, the Langmuir monolayer technique was applied. The monolayers were spread onto two different subphases, *i.e.*, TE buffer (pH 7.4) and 125 mM NaOAc buffer (pH 5.2), respectively. The Π was

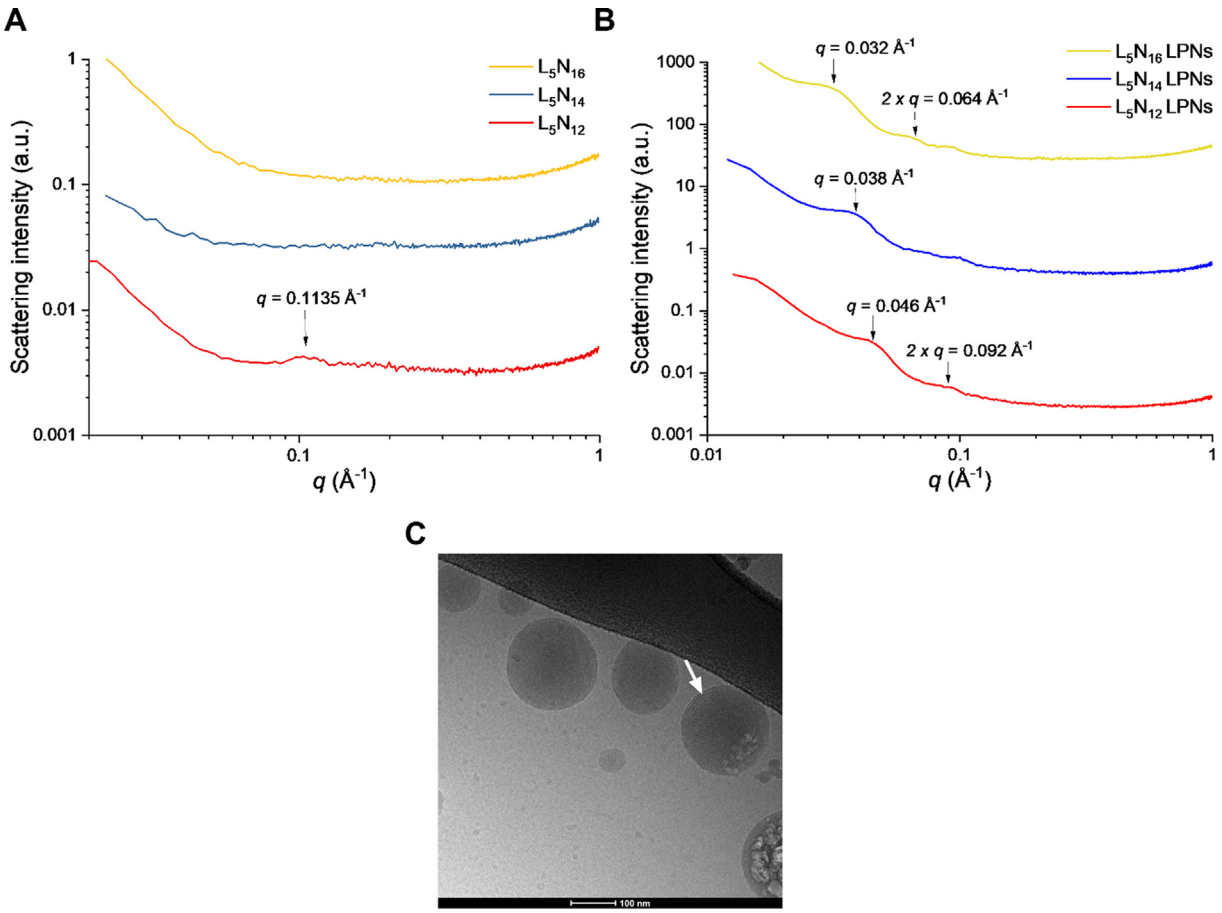

Fig. 4. Effect of chain length on structural properties. **A:** Representative SAXS diffraction patterns of lipoplexes composed of siRNA and L_5 with varying chain length [L_5N_{12} (red), L_5N_{14} (blue), and L_5N_{16} (yellow)] at a lipidoid:siRNA ratio of 15:1 in TE buffer at 20 °C. The arrow marks a peak at a *q*-value of 0.1135 $Å^{-1}$ for L_5N_{12}. The scattering intensity on the y-axis has been shifted vertically for improved visibility. **B:** Representative scattering patterns of siRNA-loaded LPN formulations containing L_5N_{12} (red), L_5N_{14} (blue), and L_5N_{16} (yellow), respectively, at a lipidoid:siRNA ratio of 15:1 and a lipidoid content of 15 % (w/w) in TE buffer measured at 20 °C. Lamellar phase first and second order reflections can be seen for L_5N_{12}-modified LPNs at *q*-values of 0.046 $Å^{-1}$ and 0.092 $Å^{-1}$ and for L_5N_{16}-modified LPNs at 0.032 $Å^{-1}$ and 0.064 $Å^{-1}$, respectively. There is one reflection at 0.038 $Å^{-1}$ for L_5N_{14}-modified LPNs, corresponding to a repeat distance of 155 Å, but there is no clear second order reflection. **C:** Representative cryo-TEM image of siRNA-loaded, L_5N_{16}-modified LPNs prepared at an L_5N_{16}:siRNA ratio of 15:1 and an L_5N_{16} content of 15 % (w/w). The arrow marks concentric lipid bilayers enclosing an electron-dense core. (For interpretation of the references to colour in this figure legend, the reader is referred to the web version of this article.)

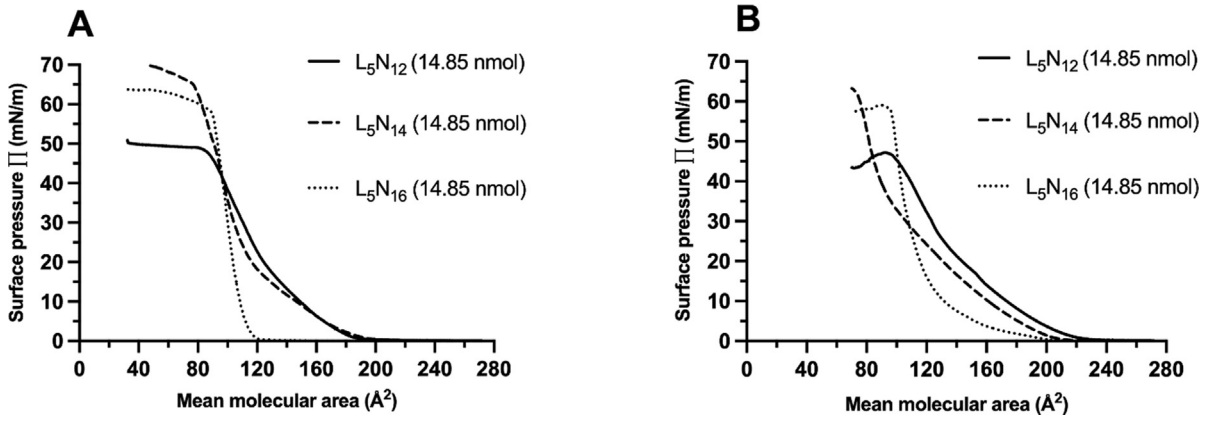

Fig. 5. Langmuir isotherms of L_5 monolayers are affected by the chain length and the pH of the buffer subphase at 22 °C. **A:** Isotherms of L_5N_{12} (solid line), L_5N_{14} (dashed line), and L_5N_{16} (dotted line) monolayers at pH 7.4. **B:** Reducing the pH to 5.2 results in expanded monolayers, as indicated by an increase in *A* of L_5N_{12} (solid line), L_5N_{14} (dashed line), and L_5N_{16} (dotted line), in the gas phase to LE phase, specifically around a mean molecular area of 200 $Å^2$. Isotherms represent mean values of 3–4 independent compressions ($N = 3$ for L_5N_{12}, and $N = 4$ for L_5N_{14} and L_5N_{16}).

measured as a function of *A* (*Π-A* isotherms) at 22 °C upon monolayer compression. The lack of any apparent phase transition in the isotherms for L_5N_{12} suggests that L_5N_{12} exists in the LE phase at 22 °C (Fig. 5A). In contrast, L_5N_{14} monolayers appeared to be in the solid (S) phase, in addition to LE and LC phases, while L_5N_{16} mostly exhibited an LC and S phase (Fig. 5A) [17]. It is evident from

Table 1
Surface pressure ($\Pi_{collapse}$) and mean molecule area at the collapse point ($A_{collapse}$), and the limiting molecule area (A_{lim}), for L_5N_{12}, L_5N_{14}, and L_5N_{16} monolayers on two different subphases at 22 °C: 10 mM TE buffer (pH 7.4) or 125 mM NaOAc buffer (pH 5.2).[a]

Monolayer	$\Pi_{collapse}$ (mN/m)		$A_{collapse}$ (Å^2)		A_{lim} (Å^2)	
	pH 7.4	pH 5.2	pH 7.4	pH 5.2	pH 7.4	pH 5.2
L_5N_{12}	48.9 ± 0.2[b***]	47.1 ± 0.5[e***]	83 ± 3	93 ± 2[f***]	146 ± 2[d***]	166 ± 3[g***]
L_5N_{14}	65.4 ± 1.2[b***]	63.3 ± 0.8[e***]	79 ± 5	71 ± 3	113 ± 8	110 ± 3
L_5N_{16}	57.7 ± 1.2[b***]	58.1 ± 0.9[e***]	91 ± 4 [c*]	95.4 ± 0.5[f***]	108 ± 4	116.0 ± 1.3

[a] Results denote mean values ± SD (n = 3–4). Statistically significant differences within each of the three parameters at pH 7.4 or pH 5.2 are indicated: *p < 0.05, and ***p < 0.001.
[b] Significant differences in $\Pi_{collapse}$ between chain lengths (p < 0.001).
[c] Significant differences in $A_{collapse}$ between chain lengths (p < 0.05, as compared to L_5N_{14}).
[d] Significant difference in A_{lim} between chain lengths (p < 0.001, as compared to L_5N_{14} and L_5N_{16}).
[e] Significant difference in $\Pi_{collapse}$ between chain lengths (p < 0.001).
[f.] Significant difference in $A_{collapse}$ between chain lengths (p < 0.001, as compared to L_5N_{14}).
[g] Significant difference in A_{lim} between chain lengths (p < 0.001, as compared to L_5N_{14} and L_5N_{16}).

the Π-A isotherms that L_5N_{14} and L_5N_{16} monolayers collapse at significantly (p < 0.001) higher surface pressures (65.4 ± 1.2 mN/m and 57.7 ± 1.2 mN/m, respectively, Table 1) than L_5N_{12} monolayers (48.9 ± 0.2 mN/m, Table 1) at a subphase pH of 7.4.

The pH of the subphase displayed a pronounced influence on the interfacial behavior of L_5N_{12} monolayers (Fig. 5B). The A_{lim} increased from 146 ± 2 Å^2 to 166 ± 3 Å^2 when the pH was reduced from 7.4 to 5.2, which was accompanied by a decrease in Π at the collapse point from 48.9 ± 0.2 mN/m to 47.1 ± 0.5 mN/m (Table 1). Interestingly, at pH 7.4, the $A_{collapse}$ of L_5N_{12} monolayers was significantly lower (p < 0.05) than the $A_{collapse}$ of L_5N_{16} monolayers, but almost identical to the $A_{collapse}$ of L_5N_{14} monolayers (Table 1), while at pH 5.2, the A_{lim} of L_5N_{12} monolayers was significantly (p < 0.001) higher than the A_{lim} of L_5N_{14} and L_5N_{16} monolayers.

3.7. L_5N_{12} monolayers interact with siRNA present the subphase in a pH-dependent way

To investigate the interaction between siRNA and L_5N_{12}, L_5N_{12} monolayers (14.84 nmol) were spread onto buffer subphases containing increasing amounts of siRNA (9.76, 14.7, 19.6 and 39.2 nmol, respectively). Increasing the content of siRNA up to 19.6 nmol in the TE buffer subphase (pH 7.4) did not cause an appreciable increase in A_{lim} relative to neat L_5N_{12} monolayers, but the addition of 39.2 nmol siRNA resulted in a shift of the isotherm towards the right. However, this shift did not affect $\Pi_{collapse}$ (Fig. 6A), suggesting that siRNA interacts with the headgroup of L_5N_{12} at pH 7.4 in a way that affects the lateral movement of L_5N_{12} in the monolayer, but does not influence monolayer packing. It also suggests that siRNA interacts with the cationic monolayer and causes steric repulsion.

Increasing the siRNA content (9.76, 14.6, 19.6, and 78.2 nmol) in the NaOAc buffer subphase (pH 5.2) caused an increase in both $\Pi_{collapse}$, $A_{collapse}$, and A_{lim} of L_5N_{12} monolayers, compared to the neat L_5N_{12} monolayers (Fig. 6B and 6C). Hence, the $\Pi_{collapse}$ of the monolayer appears to increase with an increase in siRNA concentration in the NaOAc buffer subphase (pH 5.2), while remaining relatively constant for L_5N_{12} monolayers on TE buffer subphase (pH 7.4) (Fig. 6C). This shows that the interaction between L_5N_{12} and siRNA is much stronger at pH 5.2 than at pH 7.4. The increase in $\Pi_{collapse}$ of L_5N_{12} monolayers appeared to plateau (around 50 mN/m) at 19.7 nmol siRNA in the NaOAc subphase, resulting in an A_{lim} of 180 Å^2 (Fig. 6B and 6C). Similar values were obtained when 78.3 nmol siRNA was added, suggesting that only a finite amount of siRNA can interact with the cationic L_5N_{12} monolayer, and excess siRNA remains in the subphase. Interestingly, the A_{lim} value was approx. 143 Å^2 when 19.6 nmol siRNA was present in the subphase at pH 7.4, but increased to almost 170 Å^2 when the siRNA content was increased to 39.6 nmol (Fig. 6A).

3.8. Thermotropic phase behavior

The thermotropic phase behavior of selected formulations was analyzed by using DSC. Non-loaded liposomes composed of L_5N_{12}, L_5N_{14}, and L_5N_{16}, respectively, were prepared by microfluidic mixing, and then analyzed to determine the T_m and ΔH of the phase transition. In addition, L_5N_{12}-, L_5N_{14}-, and L_5N_{16}-modified LPNs loaded with siRNA were prepared to investigate the effect of polymer and siRNA on the thermal behavior, while non-loaded, L_5N_{16}-modified LPNs served as control. A clear thermal event was observed at 40.8 °C for L_5N_{16} liposomes with a ΔH of 123.8 kJ/mol (Fig. 7A). This is attributed to a main phase transition from an ordered gel phase to a liquid disordered phase. The slight fronting at the beginning of the thermal event may be attributed to the presence of impurities (*e.g.*, L_4N_{16}). The ΔH associated with the phase transition of L_5N_{16} is relatively high, as compared to the ΔH seen for phosphatidylcholines with two acyl chains [18]. This could be due to the presence of five alkyl chains. The small exothermic peak at approx. 52 °C may be attributed to the transition to a micellar phase. In contrast, there were no apparent thermal events in the thermograms for L_5N_{12} and L_5N_{14} liposomes. This suggests that their T_m is below room temperature, and hence the membrane bilayers are already in the liquid disordered phase.

The thermal event in the thermogram of PLGA nanoparticles in the temperature range of approx. 35–40 °C (Fig. 7B) is attributed to the glass transition of PLGA from a solid, glassy state to a rubbery state [19]. This step change could also be a result of the presence of PVA on the surface of the LPNs [20]. However, there is a shift in shape and position of the thermal event when PLGA is incorporated into siRNA-loaded L_5N_{12}-modified LPNs and L_5N_{14}-modified LPNs (Fig. 7B). For siRNA-loaded, L_5N_{16}-modified LPNs, a sharp peak appears at a T_m of 53.9 °C with a ΔH of 19.9 kJ/mol (Fig. 7B). This peak is presumably the phase transition of the L_5N_{16} component of the LPNs.

To investigate whether siRNA has an effect on the phase transition of L_5N_{16}-modified LPNs, non-loaded, L_5N_{16}-modified LPNs were analyzed as well (Fig. 7C). Non-loaded LPNs showed a similar shift in the L_5N_{16} phase transition to 51.4 °C with a ΔH of 22.1 kJ/mol, which is much lower than that determined for non-loaded L_5N_{16} liposomes (123.8 kJ/mol). It is assumed that the shift in the peak position is due to interaction between L_5N_{16} and PLGA, where L_5N_{16} forms a monolayer on the surface of a PLGA core, through hydrophobic interactions. The thermogram also shows that siRNA does interact with the components of the LPNs and has an effect on the T_m of the phase transition, which is increased to 53.9 °C.

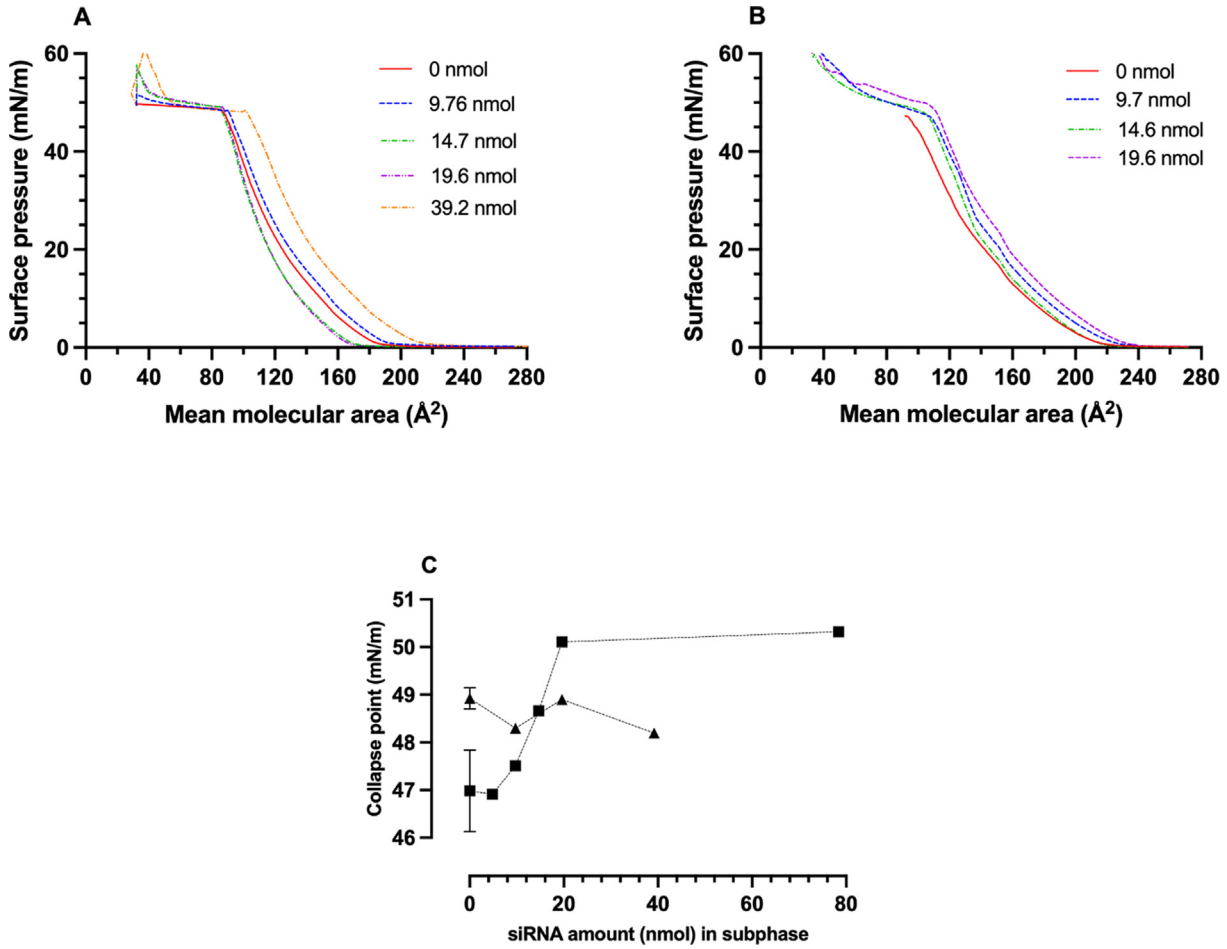

Fig. 6. L_5N_{12} monolayers interact with siRNA present the subphase in a pH-dependent manner. **A:** A general siRNA concentration-dependent increase in $A_{collapse}$ was observed for L_5N_{12} monolayers spread onto TE-buffer (pH 7.4) subphases. **B:** A general siRNA concentration-dependent increase in $\Pi_{collapse}$, $A_{collapse}$, and A_{lim} was observed for L_5N_{12} monolayers on NaOAc buffer subphases. **C:** Increase in the stability of L_5N_{12} monolayers at pH 5.2 (squares) when siRNA was added to the subphase, as indicated by an increase in $\Pi_{collapse}$, as compared to monolayers at pH 7.4 (triangles), for which addition of siRNA did not affect $\Pi_{collapse}$. Isotherms represent means of 1–3 independent compressions (N = 3 for 0 nmol siRNA, while N = 1 for > 0 nmol siRNA in the subphase). A content 39.2 nmol of siRNA in the NaOAc buffer subphase was not tested due to sample quantity usage constraints.

3.9. FTIR spectroscopy

Concentrated nanoparticle dispersions were studied further by using ATR-FTIR spectroscopy to investigate the lipid packing state by comparison with bulk PLGA and L_5N_{12}. The FTIR absorption features were characterized in the wavenumber region from 800 to 1900 cm^{-1} and 2600 to 3400 cm^{-1}, respectively, because the major functional groups of PLGA and L_5N_{12} are responsive in these two regions (Fig. 8A and B). For bulk PLGA, one of the strongest absorbance bands was apparent at 1757 cm^{-1} (Fig. 8A), which is attributed to the symmetric stretching vibrations of the ester carbonyl groups [21,22]. Stretching bands from the asymmetric and symmetric ester vibrations were also identified between 1000 and 1300 cm^{-1} with maxima at 1089, 1181, and 1272 cm^{-1} [21]. The weaker absorption band at 1386 cm^{-1} is due to the wagging and scissoring vibrations of the saturated C—H bonds. The band at 1457 cm^{-1} represents the scissoring vibration of the methyl groups C—H [23,24]. These bands were also characteristic for the siRNA-loaded LPNs (Fig. 8A), which suggests that the polymer structure is not affected by incorporation of L_5N_{12}.

Each L_5N_{12} molecule contains five amide groups and three tertiary amine groups. However, due to the weak polarity of C—N bonds, the tertiary amines all display weak-intensity stretching peaks in the range from 1020 to 1250 cm^{-1}, while several strong absorption bands arising from amides are present in the range from 1400 to 1700 cm^{-1} (Fig. 8A). With increasing L_5N_{12} content within the LPNs (from 5 % to 50 %), the absorption peaks at 1544 and 1640 cm^{-1} became more prominent (Fig. 8C, red arrows), which can be attributed to the C=O stretching of the secondary amide groups of L_5N_{12}. In addition, the intensity of the absorption peaks at 2852 and 2923 cm^{-1} also displayed a pronounced increase upon increasing the L_5N_{12} content (Fig. 8D, blue arrows), which can be attributed to the C—H stretching in the alkyl chains. Hence, these bands are useful fingerprints of the L_5N_{12} component of LPNs.

The FTIR spectrum of L_5N_{12}-siRNA lipoplexes provides interesting information. The dominant bands of L_5N_{12} are in the 1500–1700 cm^{-1} region (amide I and II, Fig. S10). In solution, siRNA adopts an A-RNA form displaying characteristic absorption bands at 811, 860, 913, and 1238 cm^{-1} [25], and an additional peak at approximately 1706 cm^{-1}, corresponding to the C=O vibration of guanine (Fig. S10). In contrast, the characteristic bands at 811 and 864 cm^{-1} disappeared for the siRNA-L_5N_{12} lipoplexes (Fig. S10), which suggest that the RNA helix may be partially unfolded. The bands at 913, 970, and 995 cm^{-1} in the FTIR spectra shifted towards higher wavenumbers, which can be a result of the interaction between L_5N_{12} and 2′-OH groups of the ribose groups in RNA. For A-RNA in solution, the characteristic band at 1238 cm^{-1} can be assigned to the asymmetric stretching vibrations of the

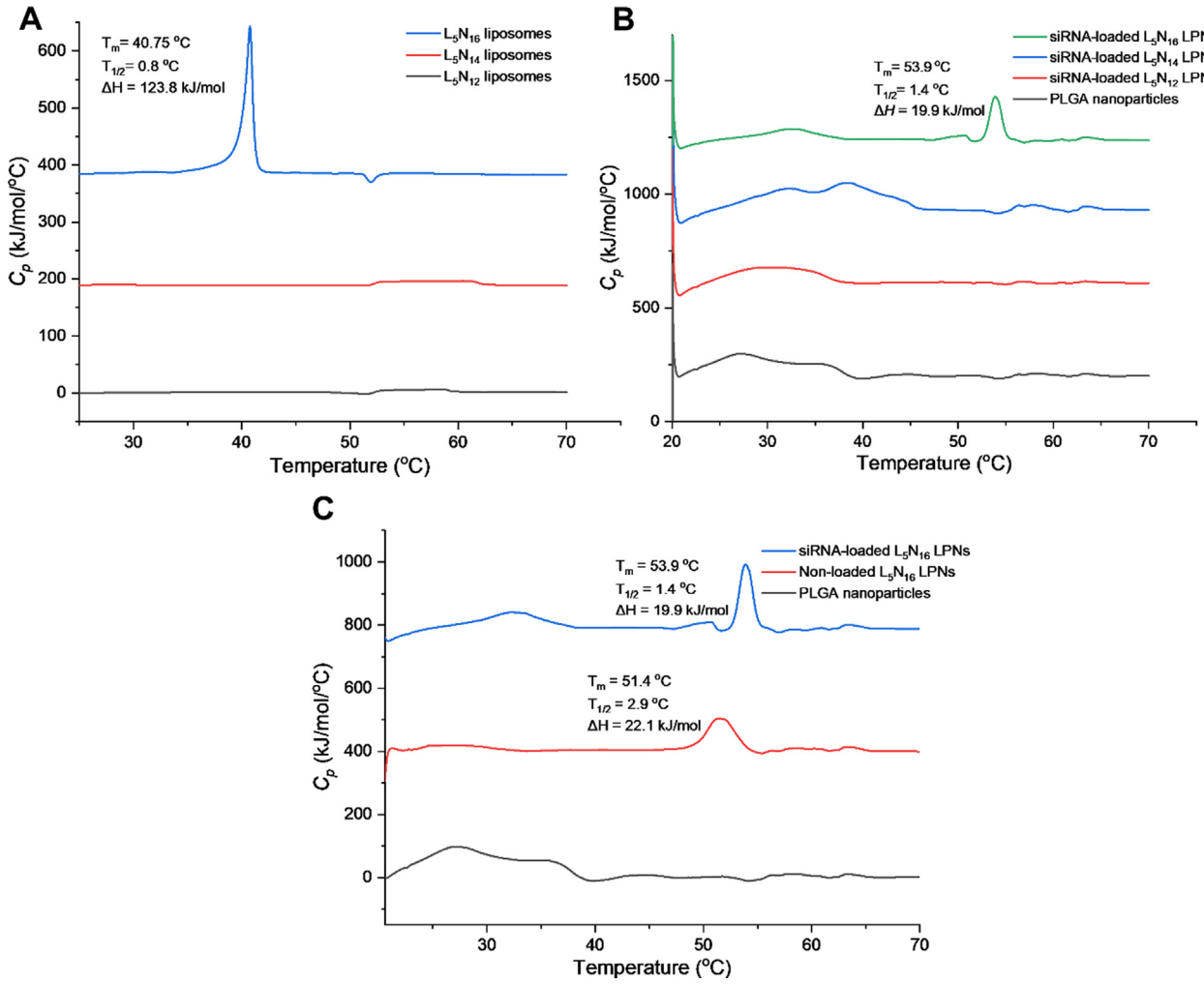

Fig. 7. Thermotropic phase behavior. **A:** Effect of chain length on the thermotropic phase behavior of liposomes. Representative DSC thermograms for L_5N_{12} (black), L_5N_{14} (red), and L_5N_{16} (blue) liposomes in NaOAc buffer prepared by using microfluidic mixing. For L_5N_{16}, a pronounced gel-to-liquid disordered phase transition is observed at 40.8 °C. **B:** DSC thermograms of siRNA-loaded, L_5N_{12}-modified LPNs (red), L_5N_{14}-modified LPNs (blue), and L_5N_{16}-modified LPNs (green) are compared to the thermogram of PLGA nanoparticles (black). **C:** DSC thermograms of non-loaded (red) and siRNA-loaded (blue), L_5N_{16}-modified LPNs, as compared to that of PLGA nanoparticles (black). The thermograms have been shifted vertically for better visibility. (For interpretation of the references to colour in this figure legend, the reader is referred to the web version of this article.)

phosphate ester groups. After lipoplex formation with L_5N_{12}, the band at 1238 cm^{-1} shifted towards shorter wavenumbers of approximately 1201 cm^{-1}, which indicates an alteration of the A-RNA structure (25).

4. Discussion

The design of safe and efficient delivery systems for nucleic acid-based therapeutics is essential for their translation into approved medicines. Elucidation of the nanoscale structure of these delivery systems, specifically nanoparticles, may facilitate their optimization via determination of possible structure–activity relationships. Here, the structure of LPNs was studied by employing several analytical techniques, as well as by comparison to the structure of various control formulations. Based on these observations, a presumed structure of LPNs is proposed.

The critical packing parameter of L_5N_{12} was calculated, using the A_{lim} of the monolayer isotherms, to be 0.77, which suggests that L_5N_{12} is likely to adopt a lamellar phase upon dispersion in aqueous medium, which is in accordance with our experimental findings: The SAXS data, polarized light microscopy images, and DSC thermograms show that L_5N_{12} self-assembles into a lamellar phase in the liquid crystalline state with a lamellar repeat distance of 38 Å in the fully hydrated state (Figs. 1 and 7). In comparison, the phospholipid 1,2-dilauroyl-*sn*-glycero-3-phosphatidylcholine with comparable chain length also adopts a lamellar structure and exhibits a repeat distance of 59 Å with a bilayer thickness of 33 Å in the fluid and fully hydrated state. Manufacture of non-loaded L_5N_{12} liposomes using microfluidic mixing resulted in unilamellar vesicles (Fig. 2A and B). This unilamellar structure is presumably a result of repulsive electrostatic interactions between the bilayers at the low pH of the NaOAc buffer (pH 5.2), rendering the hydrophilic headgroup of L_5N_{12} fully protonated. In amphiphilic systems dispersed in water, electrostatic repulsion between headgroups, as well as the osmotic pressure that the water exerts on the membranes, is an important determinant of the interbilayer distance [26]. When the L_5N_{12} headgroups are fully ionized, it is likely that the repulsion between the cationic headgroups prevents formation of concentric bilayers.

In contrast, cryo-TEM images suggest that lipoplexes of siRNA and L_5N_{12} prepared in TE buffer form concentric lipid bilayers (Fig. 2E and F). The SAXS diffraction patterns revealed a repeat distance of 55 Å, which may be attributed to an interaxial alignment

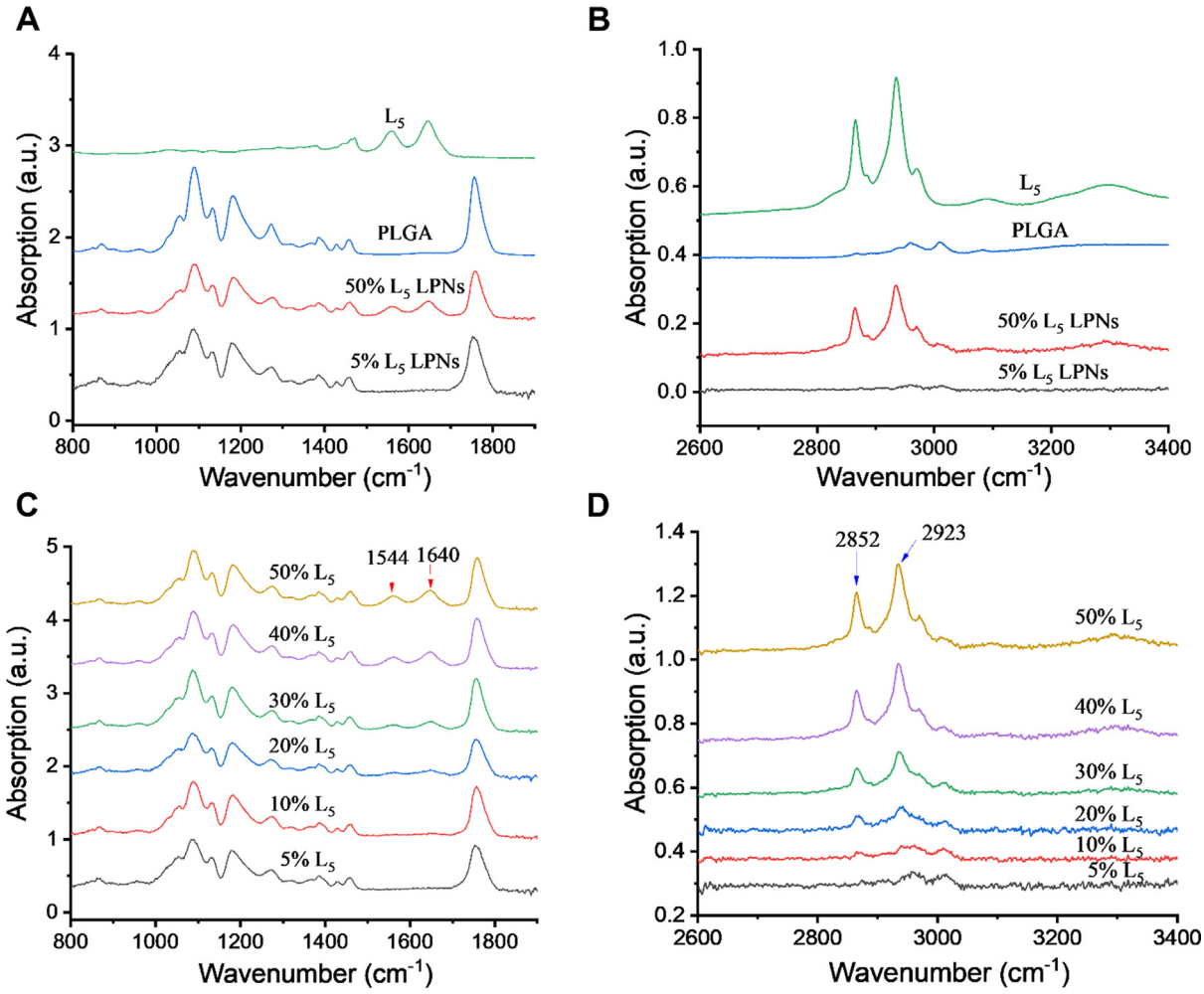

Fig. 8. A-B: FTIR spectra of siRNA-loaded LPNs containing 5 % L_5N_{12} (black) and 50 % L_5N_{12} (red) and their constituents [bulk L_5N_{12} (green) and bulk PLGA (blue)] in the region from 800 to 1900 cm^{-1} (**A**), and 2600–3400 cm^{-1} (**B**). **C-D:** FTIR spectra of siRNA-loaded LPNs with varying L_5N_{12} content from 5 % to 50 % in the region from 800 to 1900 cm^{-1} (**C**), and from 2600 to 3400 cm^{-1} (**D**). The spectra have been shifted vertically for better visibility. (For interpretation of the references to colour in this figure legend, the reader is referred to the web version of this article.)

of siRNA (Fig. 2C). The even distribution of the siRNA in the lateral space between the bilayers may be attributed to residual negative charge that has not been neutralized by interaction with the lipidoid headgroups [27]. This causes electrostatic repulsion between siRNA molecules. This may also explain the increase in A_{lim} of L_5N_{12} monolayers upon addition of siRNA to the TE buffer subphase (pH 7.4). A similar oligonucleotide lamellar phase has been observed for other lipid-based nanoparticles. In dioleoyltrimethylammoniumpropane (DOTAP)-siRNA complexes, a lamellar phase with a repeat distance of 55.9 Å (*i.e.*, almost identical to the repeat distance observed in this study) was attributed to the lateral distance arising from siRNA molecules sandwiched between lipid bilayers [28]. However, when incorporated into DOTAP-PLGA LPNs, this repeat distance decreases to 48.7 Å. This may be attributed to the presence of impurities or an effect of the PVA used for stabilization of the nanoparticles. This decrease is not observed for L_5N_{12} LPNs, where the repeat distance of the siRNA lamellar phase is largely similar to that found for L_5N_{12} lipoplexes. This can be explained by a difference in charge density. If the lipids in the bilayer exhibit a high charge density, the siRNA will pack more tightly, effectively reducing the repeat distance between the molecules. In the LPNs, the charge density of the lipid at a pH value of 7.4 could be lower than that of DOTAP, inferring that the distance between siRNA molecules is higher [29].

Due to the amorphous nature of PLGA, and the fact that non-loaded PLGA nanoparticles did not show any scattering in the investigated *q*-range (results not shown), it is reasonable to assume that all peaks present in the 1D scattering pattern of LPNs arise from structures formed by the lipidoid or siRNA. The formation of lipidoid bilayers in LPNs does not seem to be governed by siRNA, as inferred by the SAXS patterns of the non-loaded nanoparticles (Fig. 3A). Both the non-loaded as well as the loaded LPNs show first and second order lamellar reflections at L_5N_{12} contents of 15 % and higher (Fig. 3A and B). This contrasts with a report on the structure of LNPs loaded with a much larger mRNA cargo [30]. In this delivery system, it was suggested that the mRNA was important in defining the final structure that the nanoparticles adopts. The scattering pattern for mRNA-loaded nanoparticles was much more distinct, as compared to a much weaker peak in non-loaded nanoparticles. Furthermore, in LNPs composed of DLin-KC2-DMA/1,2-distearoyl-*sn*-glycero-3-phosphocholine/cholesterol/PEG-lipid (50:10:38.5:1.5 mol%), where DLin-KC2-DMA is an ionizable lipid, siRNA was found to influence the general structure of LNPs by forming a higher fraction of LNPs with a stacked bilayer structure when the loading of siRNA was increased [31]. Such a trend is not observed for L_5N_{12} LPNs, where the general structure forms, regardless of whether siRNA is incorporated or not.

The lamellar repeat distance observed for LPN bilayers (*i.e.*, the concentric lipidoid bilayers forming around the PLGA core, separated by a water layer between each of the bilayers) is significantly enlarged, as compared to the repeat distance of dispersed bulk L_5N_{12}. The repeat distance increases by 98 Å to a distance of 136 Å in LPNs with an L_5N_{12} content of 15 %, as compared to the lamellar repeat distance in dispersion (Fig. 3). This swollen lamellar phase is also observed in siRNA-loaded, DOTAP-modified LPNs and is attributed to the effect of PLGA on the bilayer [28]. However, the bilayer swelling does seem to be influenced by the preparation method. In a separate experiment, PLGA nanoparticles were coated with a layer of L_5N_{12} by using the thin-film hydration method (results not shown). The resulting LPNs were large (>300 nm) and showed a lamellar repeat distance of 38 Å, identical to the bulk L_5N_{12} dispersion. However, further cryo-TEM studies are required to support the hypothesis that LPNs are formed, rather than a dispersion of separate liposomes and PLGA nanoparticles.

In addition, for both non-loaded and siRNA-loaded LPNs, an increase in L_5N_{12} content with a decrease in PLGA content led to an increase in the calculated lamellar repeat distance (Fig. 3). However, it should be noted that the resolution attained by using benchtop SAXS could be a limitation due to the broadness of the peaks. Nonetheless, the data suggests that this change is not related to siRNA complexation. It is presently unclear why there is an increase in lamellar repeat distance when the content of L_5N_{12} is increased and the content of PLGA is decreased. Preliminary results indicate that this trend could possibly be caused by the decrease in polymer core size and be influenced by the L_5N_{12} concentration. Furthermore, the cryo-TEM images (Fig. 3D and E) suggest the existence of a variety of colloidal species (LPNs, liposomes, and lipoplexes), which could explain the peak broadening, due to sample heterogeneity. Importantly, in pioneering experiments on lipid bilayer structure, a similar increase in repeat distance was observed with an increase of the concentration of Aerosol MA; an anionic surfactant [32].

As the lamellar repeat distance is the sum of the bilayer thickness and the water layer thickness, a change in the thickness of either layer could be the cause of the increased distance. Based on cryo-TEM images of LPNs containing 70 % L_5N_{12}, this change in distance seems initially to be the result of an increase in water layer thickness, but this is inconclusive (Fig. 3D and E). Alternatively, it could be attributed to the presence of PVA as an interfacial polymer between lipid bilayers. It is possible, even with purification considered, that more PVA is retained when the L_5N_{12} concentration is increased. A study of PVA retention on PLGA nanoparticles showed that even trace amounts of residual PVA has an effect on the physical properties of the nanoparticles [33]. This increase in the content of PVA could result in larger interbilayer distances.

At an L_5N_{12} content of 5 %, the lack of clear structural peaks in the scattering patterns suggests a less uniform coating of the PLGA nanoparticles. This L_5N_{12} content is presumably not sufficient for bilayer formation, and the resulting nanoparticles possibly consist of a spherical PLGA core with a monolayer of L_5N_{12} embedded in the polymer matrix through hydrophobic interactions (Fig. 9). The appearance of lamellar reflections at higher concentrations suggest that there is a certain threshold for full coating of the PLGA core before bilayer formation can take place. Furthermore, the appearance of bilayers in cryo-TEM images is much more pronounced at an L_5N_{12} content of 70 % as compared to 15 %. However, the general structure of concentric lipid bilayers surrounding an electron-dense core does not seem to change, when the L_5N_{12} content is increased.

Complexation of nucleic acids has been reported to decrease the lamellar repeat distance in monoolein-based lipoplexes [34]. Furthermore, in DOTAP-based LPNs, it is reported that the ratio of nucleic acid to lipid seems to affect the bilayer thickness, with a relative increase in the content of nucleic acid leading to a smaller lamellar repeat distance. This is explained by the electrostatic complexation between the negatively charged siRNA and positively charged lipid, where the result of neutralizing the positive charge on the headgroups is reduced interbilayer repulsion. This reduced repulsive electrostatic force causes compression of the bilayer, which becomes more compact, and therefore shows a smaller repeat distance. This did not seem to be the case for LPNs, which displayed a relatively constant repeat distance when the ratio of siRNA to L_5N_{12} was varied (Fig. 3F). This suggests that at pH 7.4, there insufficient residual positive charge on the ionizable L_5N_{12} to have an impact on the interbilayer distance, and that the alkyl chains and the water layer thickness are more important determinants of lamellar repeat distance.

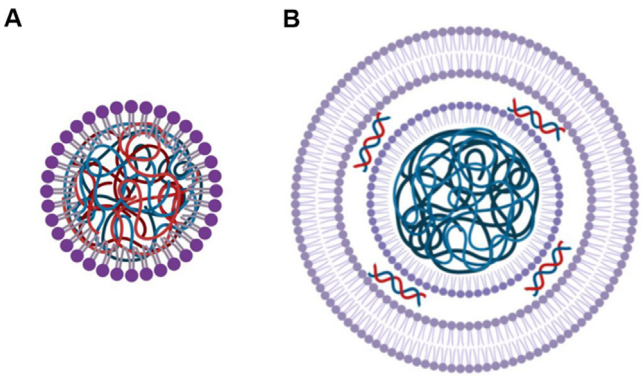

Fig. 9. A: Illustration of the proposed formation of a monolayer of L_5N_{16} on a PLGA core through hydrophobic interactions. **B:** LPNs based on L_5N_{12} and L_5N_{14} form a core–shell structure. PLGA acts as the hydrophobic core matrix, with a monolayer of L_5 on the surface. Concentric lipid bilayers form around this core, and siRNA molecules are equally spaced and sandwiched in-between these bilayers through attractive electrostatic interactions with the amine lipid headgroups. Created with BioRender.com.

LPNs based on L_5N_{14} and L_5N_{16} show similar results to L_5N_{12} LPNs. They all possess a spherical nanoparticle morphology, and bilayer formation is evident (Fig. 4). This spherical electron-dense LPN structure, as resolved using cryo-TEM, is similar to that reported for N^1,N^3,N^5-tris(2-aminoethyl)benzene-1,3,5-tricarboxamide (TT3)-based LPNs with a proposed hydrophobic PLGA core [35].

The increase in lamellar repeat distance associated with these LPNs can therefore only be explained by the increase in the chain length of the lipidoids. This is in accordance with lamellar repeat distances of phosphatidylcholine lipids with variable chain lengths reported in the literature [36]: For example, at a chain length of 12 carbon atoms, the repeat distance was 30.5 Å, and for a 16 carbon length tail, the repeat distance was 37 Å. The cationic headgroup of L_5 contains both secondary and tertiary amines, and their degree of protonation is highly dependent on the pH, which eventually may affect the interaction with siRNA. The Langmuir monolayer technique was used to characterize this interaction further. Monolayers of neat lipidoids were spread on two different subphases of pH 7.4 and 5.2. L_5N_{12}, L_5N_{14}, and L_5N_{16} have the same headgroup, but differ by two carbon atoms per alkyl chain, eventually resulting in a difference of 10 and 20 additional carbon atoms per molecule, respectively, relative to L_5N_{12}. As expected, increasing the alkyl chain length resulted in a decrease in the A_{lim} and an increase in the $\Pi_{collapse}$ due to stronger van der Waal forces between the alkyl chains at a constant pH. The same has been observed for saturated phospholipids when the acyl chain length was increased from 14 to 18 carbon atoms [37]. This highlights that L_5N_{14} and L_5N_{16} form more stable monolayers than L_5N_{12}, most likely due to stronger

van der Waal forces between their longer alkyl chains [11,38,39]. At pH 5.2, electrostatic repulsive interactions between the cationic headgroups are stronger, as evident from the expansion of the isotherms, which is indicated by an overall shift of the isotherms toward higher A_{lim} values (Fig. 5B). A comparable pH-dependent increase in A_{lim} and monolayer expansion have also been observed for other cationic lipids [40,41].

Nucleic acids are generally deprotonated and hence negatively charged at physiologically relevant pH values due to their low pK_a values. Interactions between monolayers and molecules present in the subphase occur due to electrostatic and hydrophobic interactions, as well as hydrogen bonding [42]. At a subphase pH of 7.4, increasing the content of siRNA in the subphase (up to 19.6 nmol) did not cause an appreciable increase in the A_{lim}, while at 39.6 nmol siRNA, the A_{lim} was increased, which suggests that siRNA interacts with the headgroup of L_5N_{12} in a way that affects the lateral movement of L_5N_{12} in the monolayer, but does not influence monolayer packing. It also suggests that siRNA interacts with the cationic monolayer and causes steric repulsion due to the siRNA molecules. This is in agreement with data reported for cationic lipid-DNA interactions [44]. This shows that the interaction between L_5N_{12} and siRNA is much stronger at pH 5.2 than at pH 7.4. At pH 5.2, the headgroups are more loosely packed than at pH 7.4 due to a higher degree of protonation [44]. When siRNA is added to the subphase, the area occupied by the headgroups of L_5N_{12} at pH 5.2 is significantly larger ($p < 0.01$) than the area occupied at pH 7.4. In both cases, an interesting observation was the difference in $A_{collapse}$ when the content of siRNA in the subphase was 9.7 or 19.6 nmol (Fig. 6B). It was expected that $A_{collapse}$ would generally increase with an increase in the content of siRNA, but this is not the case here. Previous reports suggest that monolayers of cationic lipids can be condensed to a greater extent in the presence of a specific amount of DNA [43]. The subphase pH and the content of siRNA in the subphase affected the A_{lim} values of the monolayer (Fig. 6A and B). At a pH of 7.4, the increase in A_{lim} might primarily be due to incorporation of siRNA in the monolayers causing steric repulsion, but only secondarily due to protonation of the headgroups of the L_5N_{12} monolayer. However, at a pH of 5.2, the monolayer is expanded due to protonation of the headgroups, in addition to steric repulsion caused by siRNA molecules, resulting in higher A_{lim} values compared to the ones at pH 7.4. Interestingly, at pH 5.2, the $\Pi_{collapse}$ increased with increasing content of siRNA in the subphase, which may contribute to stabilizing the monolayer by reducing repulsive electrostatic headgroup interactions. For a similar system, the $\Pi_{collapse}$ of a negatively charged monolayer increased when a positively charged poly(amidoamine) dendrimer was added to the subphase [45]. No further increase in $\Pi_{collapse}$ was observed beyond 19.6 nmol siRNA in the subphase at pH 5.2, which might be due to saturation of the siRNA binding sites of the monolayer. Several studies indicate that the N/P ratio is a useful parameter in the optimization studies of LNPs [46–48]. However, to describe lipid-like materials, weight ratios are typically used [35,49,50], most likely due to the multiple pK_a centers in the lipidoid molecule. This makes it difficult to accurately assess the mechanistic interactions between the lipid-like materials and siRNA, because the protonation state cannot be directly related to the buffer pH.

Thermal analysis of LPNs provides an indication of the interactions between polymer, lipid, and siRNA (Fig. 7). The incorporation of siRNA had a pronounced effect on the phase transition temperature of L_5N_{16} by increasing the T_m. A similar shift in the T_m was observed in a study of lipid-DNA complexes [51]. This effect on T_m was explained by the fact that condensation of nucleic acids with the positively charge lipid headgroups causes a shielding of charge in the cationic lipid bilayer. This results in stabilization of the lipid chains as charged lipid headgroups favor an increased surface area that is brought about by chain melting. Due to reduced electrostatic repulsive interactions between the headgroups of L_5N_{16} bilayers, the T_m increases. However, the increase in T_m measured for L_5N_{16}-modified LPNs is smaller than that observed for lipid-DNA complexes. This may be explained by the low headgroup charge density of L_5N_{16} bilayers at pH 7.4. Furthermore, for non-loaded LPNs, the addition of PLGA resulted in a large increase in the T_m of 10.7 °C. This could be attributed to the formation of strong hydrophobic interactions at the surface of a polymeric core. Similar shifts in T_m of lipid-modified PLGA formulations were observed for dimethyldioctadecylammonium-modified PLGA formulations [22]. Thermograms were analyzed for formulations with low PLGA content and low lipid content. Both formulations showed an increase in T_m, which was higher with increased PLGA content.

From FTIR spectrometric data (Fig. 8), the characteristic absorption bands of both siRNA and L_5N_{12} were markedly changed after mixing of L_5N_{12} with siRNA, which confirms strong interactions and the formation of lipoplex structures in aqueous solution. However, for the siRNA-loaded LPNs, FTIR absorption of siRNA cannot be resolved due to the low siRNA content.

The data suggests that LPNs adopt a core–shell structure, wherein PLGA constitutes a hydrophobic polymer core, with a monolayer of L_5 formed around it through hydrophobic interactions (Fig. 9). At certain concentrations of L_5N_{12}, concentric lipid bilayers are formed, in between which siRNA is sandwiched equidistantly. Similar conclusions have been drawn in the literature for other types of hybrid formulations. In a study on lecithin-PLGA hybrid nanoparticles, a core–shell structure was proposed [52]. The nanoparticles were stained with uranyl acetate, and then a lipid shell could be observed with TEM. However, further analysis by using confocal laser scanning microscopy suggested a hollow water-filled core within the PLGA [53]. This does not seem to be the case for the LPNs analyzed in the present study, wherein a matrix PLGA core is indicated to be present. Similarly, TT3-modified LPNs are also proposed to display a core–shell structure, based on cryo-TEM images [35]. Furthermore, studies on the interaction of lipid bilayers with latex show that lipid bilayers, as well as lipid monolayers, can form around the polymer core [54]. Herein, it was suggested that a lipid bilayer forms initially on the surface, and then rearranges into a monolayer due to the hydrophobic interactions between the polymer and the lipid chains. This indicates that the formation of a monolayer is thermodynamically favorable, even if some latex cores had bilayers formed around them. The DSC data provided on the interaction between L_5N_{16} and PLGA could be a preliminary indicator for the formation of a monolayer, rather than a bilayer, around the PLGA core.

5. Conclusions

It is evident that L_5N_{12} forms a lamellar liquid crystalline phase in bulk dispersion. In contrast, non-loaded L_5N_{12} liposomes adopt flexible multi-shaped unilamellar vesicles, whereas complexation with siRNA results in lipoplexes consisting of concentric lipid bilayers in the liquid crystalline phase. The LPN nanostructure seems to fit with a core–shell model, where PLGA constitutes the hydrophobic core. Presumably, a monolayer of lipidoid covers the surface of the PLGA core as a shell, possibly as a result of hydrophobic interactions between the lipidoid alkyl chains and the PLGA core, which is evident from the shift in thermal behavior of PLGA and L_5N_{16} upon incorporation into LPNs. SAXS data and cryo-TEM images show that the PLGA core is surrounded by layers of concentric lipid bilayers formed by L_5N_{12}. This core–shell structure adopted by the LPNs is clearly affected by the loading of siRNA, but the lamellar repeat distance is independent of siRNA loading.

Furthermore, the lamellar repeat distance increases with an increasing L_5N_{12} content and lipidoid chain length, and L_5N_{14} and L_5N_{16} LPNs most likely adopt a similar structure as L_5N_{12} LPNs. Collectively, the characterization data infer that siRNA-loaded LPNs adopt a core–shell structure. However, further studies are required to improve our understanding of the internal morphology of these nanostructures.

6. Funding sources

We gratefully acknowledge the support from the Innovative Medicines Initiative Joint Undertaking under grant agreement No. 115363 resources which are composed of financial contribution from the European Union's Seventh Framework Programme (FP7/2007–2013) and EFPIA companies' in kind contribution. This project has received funding from the European Union's Seventh Framework Programme for research, technological development and demonstration under grant agreement No. 600207. We are also grateful to the Lundbeck Foundation – Denmark (R219-2016-908), the Novo Nordisk Foundation – Denmark (grant no. NNF17OC0026526), the Independent Research Fund, Denmark, Technology and Production Sciences (Grant No 9041-00198B), and the Hørslev-Fonden – Denmark for financial support. We are grateful to the Jiangsu Government for the Scholarship for Overseas Studies to Yibang Zhang.

Notes.

The authors declare no competing interests.

CRediT authorship contribution statement

Anas Aljabbari: Investigation, Formal analysis, Visualization, Writing – original draft. **Abhijeet Girish Lokras:** Investigation, Formal analysis, Visualization, Writing – original draft. **Jacob Judas Kain Kirkensgaard:** Methodology, Formal analysis, Resources, Writing – review & editing, Supervision. **Thomas Rades:** Methodology, Writing – review & editing, Supervision. **Henrik Franzyk:** Methodology, Investigation, Writing – review & editing, Supervision. **Aneesh Thakur:** Methodology, Writing – review & editing, Supervision. **Yibang Zhang:** Methodology, Investigation, Formal analysis, Visualization, Writing – original draft, Supervision, Funding acquisition. **Camilla Foged:** Conceptualization, Methodology, Writing – review & editing, Supervision, Project administration, Funding acquisition.

Data availability

Data will be made available on request.

Declaration of Competing Interest

The authors declare that they have no known competing financial interests or personal relationships that could have appeared to influence the work reported in this paper.

Acknowledgements

We are grateful to Abishek Wadhwa and Christian Janfelt for excellent technical assistance. We gratefully acknowledge Center for Integrated Microscopy at the Faculty of Health and Medical Sciences, University of Copenhagen for excellent support with cryo-TEM.

Appendix A. Supplementary material

Supplementary data to this article can be found online at https://doi.org/10.1016/j.jcis.2022.11.141.

References

[1] F. Wang, T. Zuroske, J.K. Watts, RNA therapeutics on the rise, Nat. Rev. Drug Discov. 19 (7) (2020) 441–442.
[2] A. Akinc, M.A. Maier, M. Manoharan, K. Fitzgerald, M. Jayaraman, S. Barros, S. Ansell, X. Du, M.J. Hope, T.D. Madden, B.L. Mui, S.C. Semple, Y.K. Tam, M. Ciufolini, D. Witzigmann, J.A. Kulkarni, R. van der Meel, P.R. Cullis, The Onpattro story and the clinical translation of nanomedicines containing nucleic acid-based drugs, Nat. Nanotechnol. 14 (12) (2019) 1084–1087.
[3] K. Thanki, X. Zeng, S. Justesen, S. Tejlmann, E. Falkenberg, E. Van Driessche, H. Mørck Nielsen, H. Franzyk, C. Foged, Engineering of small interfering RNA-loaded lipidoid-poly(DL-lactic-co-glycolic acid) hybrid nanoparticles for highly efficient and safe gene silencing: a quality by design-based approach, Eur. J. Pharm. Biopharm. 120 (2017) 22–33.
[4] A. Akinc, A. Zumbuehl, M. Goldberg, E.S. Leshchiner, V. Busini, N. Hossain, S.A. Bacallado, D.N. Nguyen, J. Fuller, R. Alvarez, A. Borodovsky, T. Borland, R. Constien, A. de Fougerolles, J.R. Dorkin, K. Narayanannair Jayaprakash, M. Jayaraman, M. John, V. Koteliansky, M. Manoharan, L. Nechev, J. Qin, T. Racie, D. Raitcheva, K.G. Rajeev, D.W.Y. Sah, J. Soutschek, I. Toudjarska, H.-P. Vornlocher, T.S. Zimmermann, R. Langer, D.G. Anderson, A combinatorial library of lipid-like materials for delivery of RNAi therapeutics, Nat. Biotechnol. 26 (5) (2008) 561–569.
[5] K. Thanki, D. van Eetvelde, A. Geyer, J. Fraire, R. Hendrix, H. Van Eygen, E. Putteman, H. Sami, C. de Souza Carvalho-Wodarz, H. Franzyk, H.M. Nielsen, K. Braeckmans, C.-M. Lehr, M. Ogris, C. Foged, Mechanistic profiling of the release kinetics of siRNA from lipidoid-polymer hybrid nanoparticles in vitro and in vivo after pulmonary administration, J. Control. Release 310 (2019) 82–93.
[6] M.A.A. Jansen, L.H. Klausen, K. Thanki, J. Lyngsø, J. Skov Pedersen, H. Franzyk, H. M. Nielsen, W. van Eden, M. Dong, F. Broere, C. Foged, X. Zeng, Lipidoid-polymer hybrid nanoparticles loaded with TNF siRNA suppress inflammation after intra-articular administration in a murine experimental arthritis model, Eur. J. Pharm. Biopharm. 142 (2019) 38–48.
[7] K. Thanki, X. Zeng, C. Foged, Preparation, characterization, and in vitro evaluation of lipidoid-polymer hybrid nanoparticles for siRNA delivery to the cytosol, Methods Mol. Biol. 1943 (2019) 141–152.
[8] B. Martin-Bertelsen, A. Yaghmur, H. Franzyk, S. Justesen, J.J. Kirkensgaard, C. Foged, Conserved molecular superlattices in a series of homologous synthetic mycobacterial cell-wall lipids forming interdigitated bilayers, Langmuir 32 (48) (2016) 12693–12701.
[9] T.C. Huang, H. Toraya, T.N. Blanton, Y. Wu, X-ray powder diffraction analysis of silver behenate, a possible low-angle diffraction standard, J. Appl. Cryst. 26 (1993) 180–184.
[10] P. Nordly, K.S. Korsholm, E.A. Pedersen, T.S. Khilji, H. Franzyk, L. Jorgensen, H. M. Nielsen, E.M. Agger, C. Foged, Incorporation of a synthetic mycobacterial monomycoloyl glycerol analogue stabilizes dimethyldioctadecylammonium liposomes and potentiates their adjuvant effect in vivo, Eur. J. Pharm. Biopharm. 77 (1) (2011) 89–98.
[11] M.D. Phan, K. Shin, Effects of cardiolipin on membrane morphology: a Langmuir monolayer study, Biophys. J . 108 (8) (2015) 1977–1986.
[12] C. Tanford, Micelle shape and size, J. Phys. Chem. 76 (21) (1972) 3020–3024.
[13] A. Ładniak, M. Jurak, A.E. Wiącek, Langmuir monolayer study of phospholipid DPPC on the titanium dioxide–chitosan–hyaluronic acid subphases, Adsorption 25 (3) (2019) 469–476.
[14] A. Lokras, A. Thakur, A. Wadhwa, K. Thanki, H. Franzyk, C. Foged, Optimizing the intracellular delivery of therapeutic anti-inflammatory TNF-alpha siRNA to activated macrophages using lipidoid-polymer hybrid nanoparticles, Front. Bioeng. Biotechnol. 8 (2020) 601155.
[15] Y.B. Vysotsky, E.S. Kartashynska, D. Vollhardt, V.B. Fainerman, Surface pKa of saturated carboxylic acids at the air/water interface: a quantum chemical approach, J. Phys. Chem. C 124 (25) (2020) 13809–13818.
[16] C. Dormenval, A. Lokras, G. Cano-Garcia, A. Wadhwa, K. Thanki, F. Rose, A. Thakur, H. Franzyk, C. Foged, Identification of factors of importance for spray drying of small interfering RNA-loaded lipidoid-polymer hybrid nanoparticles for inhalation, Pharm. Res. 36 (10) (2019).
[17] I. Kubo, S. Adachi, H. Maeda, A. Seki, Phosphatidylcholine monolayers observed with Brewster angle microscopy and π-A isotherms, Thin Solid Films 393 (1) (2001) 80–85.
[18] M. Myers, O.L. Mayorga, J. Emtage, E. Freire, Thermodynamic characterization of interactions between ornithine transcarbamylase leader peptide and phospholipid bilayer membranes, Biochemistry 26 (14) (1987) 4309–4315.
[19] G. Liu, K. McEnnis, Glass transition temperature of PLGA particles and the influence on drug delivery applications, Polymers (Basel) 14 (5) (2022) 993.
[20] T. Congdon, P. Shaw, M.I. Gibson, Thermoresponsive, well-defined, poly(vinyl alcohol) co-polymers, Polym. Chem. 6 (26) (2015) 4749–4757.
[21] D.C. Erbetta, Synthesis and characterization of poly(D, L-Lactide-co-Glycolide) copolymer, J. Biomater. Nanobiotechnol. 03 (02) (2012) 208–225.
[22] F. Rose, J.E. Wern, P.T. Ingvarsson, M. van de Weert, P. Andersen, F. Follmann, C. Foged, Engineering of a novel adjuvant based on lipid-polymer hybrid

nanoparticles: a quality-by-design approach, J. Control. Release 210 (2015) 48–57.
[23] G. Kister, G. Cassanas, M. Vert, Morphology of poly(glycolic acid) by IR and Raman spectroscopies, Spectrochim. Acta A Mol. Biomol. Spectrosc. 53 (9) (1997) 1399–1403.
[24] G. Kister, G. Cassanas, M. Vert, Effects of morphology, conformation and configuration on the IR and Raman spectra of various poly(lactic acid)s, Polymer 39 (2) (1998) 267–273.
[25] M. Skupin, K. Sobczak, R. Zieliński, M. Kozak, The system with zwitterionic lactose-based surfactant for complexation and delivery of small interfering ribonucleic acid—a structural and spectroscopic study, Appl. Phys. Lett. 108 (21) (2016) 213701.
[26] J. Israelachvili, H. Wennerstrom, Role of hydration and water structure in biological and colloidal interactions, Nature 379 (6562) (1996) 219–225.
[27] J.O. Rädler, I. Koltover, A. Jamieson, T. Salditt, C.R. Safinya, Structure and interfacial aspects of self-assembled cationic lipid-DNA gene carrier complexes, Langmuir 14 (15) (1998) 4272–4283.
[28] S. Colombo, D. Cun, K. Remaut, M. Bunker, J. Zhang, B. Martin-Bertelsen, A. Yaghmur, K. Braeckmans, H.M. Nielsen, C. Foged, Mechanistic profiling of the siRNA delivery dynamics of lipid-polymer hybrid nanoparticles, J. Control. Release 201 (2015) 22–31.
[29] O. Farago, K. Ewert, A. Ahmad, H.M. Evans, N. Gronbech-Jensen, C.R. Safinya, Transitions between distinct compaction regimes in complexes of multivalent cationic lipids and DNA, Biophys. J . 95 (2) (2008) 836–846.
[30] M. Yanez Arteta, T. Kjellman, S. Bartesaghi, S. Wallin, X. Wu, A.J. Kvist, A. Dabkowska, N. Székely, A. Radulescu, J. Bergenholtz, L. Lindfors, Successful reprogramming of cellular protein production through mRNA delivered by functionalized lipid nanoparticles, PNAS 115 (15) (2018).
[31] J.A. Kulkarni, M.M. Darjuan, J.E. Mercer, S. Chen, R. van der Meel, J.L. Thewalt, Y. Y.C. Tam, P.R. Cullis, On the formation and morphology of lipid nanoparticles containing Ionizable cationic lipids and siRNA, ACS Nano 12 (5) (2018) 4787–4795.
[32] V. Luzzati, F. Husson, The structure of the liquid-crystalline phasis of lipid-water systems, J. Cell Biol. 12 (1962) 207–219.
[33] S.K. Sahoo, J. Panyam, S. Prabha, V. Labhasetwar, Residual polyvinyl alcohol associated with poly (D, L-lactide-co-glycolide) nanoparticles affects their physical properties and cellular uptake, J. Control. Release 82 (1) (2002) 105–114.
[34] B. Angelov, A. Angelova, R. Mutafchieva, S. Lesieur, U. Vainio, V.M. Garamus, G. V. Jensen, J.S. Pedersen, SAXS investigation of a cubic to a sponge (L3) phase transition in self-assembled lipid nanocarriers, PCCP 13 (8) (2011) 3073–3081.
[35] W. Zhao, C. Zhang, B. Li, X. Zhang, X. Luo, C. Zeng, W. Li, M. Gao, Y. Dong, Lipid polymer hybrid nanomaterials for mRNA delivery, Cell. Mol. Bioeng. 11 (5) (2018) 397–406.
[36] B.A. Lewis, D.M. Engelman, Lipid bilayer thickness varies linearly with acyl chain length in fluid phosphatidylcholine vesicles, J. Mol. Biol. 166 (2) (1983) 211–217.
[37] T. Miyoshi, S. Kato, Detailed analysis of the surface area and elasticity in the saturated 1,2-diacylphosphatidylcholine/cholesterol binary monolayer system, Langmuir 31 (33) (2015) 9086–9096.
[38] G.C. Nutting, W.D. Harkins, Pressure-area relations of fatty acid and alcohol monolayers, J. Am. Chem. Soc. 5 (1939) 1180–1187.
[39] S. Cheng, S. Li, N.T. Tsona, C. George, L. Du, Insights into the headgroup and chain length dependence of surface characteristics of organic-coated sea spray aerosols, ACS Earth Space Chem. 3 (4) (2019) 571–580.
[40] M.N. Antipina, I. Schulze, M. Heinze, B. Dobner, A. Langner, G. Brezesinski, Physical-chemical properties and transfection activity of cationic lipid/DNA complexes, ChemPhysChem 10 (14) (2009) 2471–2479.
[41] C. Symietz, M. Schneider, G. Brezesinski, H. Möhwald, DNA alignment at cationic lipid monolayers at the air/water interface, Macromolecules 37 (10) (2004) 3865–3873.
[42] B. Krajewska, P. Wydro, A. Janczyk, Probing the modes of antibacterial activity of chitosan. Effects of pH and molecular weight on chitosan interactions with membrane lipids in Langmuir films, Biomacromolecules 12 (11) (2011) 4144–4152.
[43] M.N. Antipina, I. Schulze, B. Dobner, A. Langner, G. Brezesinski, Physicochemical investigation of a lipid with a new core structure for gene transfection: 2-amino-3-hexadecyloxy-2-(hexadecyloxymethyl)propan-1-ol, Langmuir 23 (7) (2007) 3919–3926.
[44] S. Tassler, B. Dobner, L. Lampp, R. Ziółkowski, E. Malinowska, C. Wölk, G. Brezesinski, DNA delivery systems based on peptide-mimicking cationic lipids—the effect of the Co-lipid on the structure and DNA binding capacity, Langmuir 35 (13) (2019) 4613–4625.
[45] V. Tiriveedhi, K.M. Kitchens, K.J. Nevels, H. Ghandehari, P. Butko, Kinetic analysis of the interaction between poly(amidoamine) dendrimers and model lipid membranes, Biochim. Biophys. Acta Biomembr. 1808 (1) (2011) 209–218.
[46] L. Schoenmaker, D. Witzigmann, J.A. Kulkarni, R. Verbeke, G. Kersten, W. Jiskoot, D.J.A. Crommelin, mRNA-lipid nanoparticle COVID-19 vaccines: Structure and stability, Int. J. Pharm. 601 (2021) 120586.
[47] K.J. Hassett, K.E. Benenato, E. Jacquinet, A. Lee, A. Woods, O. Yuzhakov, S. Himansu, J. Deterling, B.M. Geilich, T. Ketova, C. Mihai, A. Lynn, I. McFadyen, M. J. Moore, J.J. Senn, M.G. Stanton, Ö. Almarsson, G. Ciaramella, L.A. Brito, Optimization of lipid nanoparticles for intramuscular administration of mRNA vaccines, Mol. Ther. Nucl. Acids 15 (2019) 1–11.
[48] E. Robinson, K.D. MacDonald, K. Slaughter, M. McKinney, S. Patel, C. Sun, G. Sahay, Lipid nanoparticle-delivered chemically modified mrna restores chloride secretion in cystic fibrosis, Mol. Ther. 26 (8) (2018) 2034–2046.
[49] K.T. Love, K.P. Mahon, C.G. Levins, K.A. Whitehead, W. Querbes, J.R. Dorkin, J. Qin, W. Cantley, L.L. Qin, T. Racie, M. Frank-Kamenetsky, K.N. Yip, R. Alvarez, D. W.Y. Sah, A. de Fougerolles, K. Fitzgerald, V. Koteliansky, A. Akinc, R. Langer, D. G. Anderson, Lipid-like materials for low-dose, in vivo gene silencing, PNAS 107 (5) (2010) 1864–1869.
[50] K.A. Whitehead, J.R. Dorkin, A.J. Vegas, P.H. Chang, O. Veiseh, J. Matthews, O.S. Fenton, Y. Zhang, K.T. Olejnik, V. Yesilyurt, D. Chen, S. Barros, B. Klebanov, T. Novobrantseva, R. Langer, D.G. Anderson, Degradable lipid nanoparticles with predictable in vivo siRNA delivery activity, Nat. Commun. 5 (1) (2014).
[51] R. Zantl, L. Baicu, F. Artzner, I. Sprenger, G. Rapp, J.O. Rädler, Thermotropic phase behavior of cationic lipid–DNA complexes compared to binary lipid mixtures, J. Phys. Chem. B 103 (46) (1999) 10300–10310.
[52] L. Zhang, J.M. Chan, F.X. Gu, J.-W. Rhee, A.Z. Wang, A.F. Radovic-Moreno, F. Alexis, R. Langer, O.C. Farokhzad, Self-assembled lipid–polymer hybrid nanoparticles: a robust drug delivery platform, ACS Nano 2 (8) (2008) 1696–1702.
[53] J. Shi, Z. Xiao, A.R. Votruba, C. Vilos, O.C. Farokhzad, Differentially charged hollow core/shell lipid-polymer-lipid hybrid nanoparticles for small interfering RNA delivery, Angew. Chem. Int. Ed. Engl. 50 (31) (2011) 7027–7031.
[54] A.M. Carmona-Ribeiro, M. de Moraes Lessa, Interactions between bilayer membranes and latex, Colloids Surf. A Physicochem. Eng. Asp 153 (1-3) (1999) 355–361.